Highly parameterized inversion of groundwater reactive transport for a complex field site

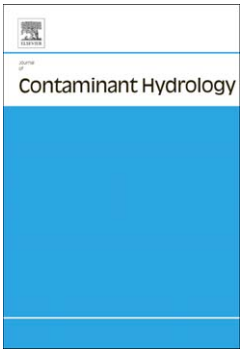

Highly parameterized inversion of groundwater reactive transport for a complex field site

Luca Carniato, Gerrit Schoups, Nick van De Giesen, Piet Seuntjens, Leen Bastiaens, Hans Sapion

PII: S0169-7722(14)00217-4
DOI: doi: 10.1016/j.jconhyd.2014.12.001
Reference: CONHYD 3077

To appear in: *Journal of Contaminant Hydrology*

Received date: 3 July 2014
Revised date: 15 October 2014
Accepted date: 1 December 2014

Please cite this article as: Carniato, Luca, Schoups, Gerrit, van De Giesen, Nick, Seuntjens, Piet, Bastiaens, Leen, Sapion, Hans, Highly parameterized inversion of groundwater reactive transport for a complex field site, *Journal of Contaminant Hydrology* (2014), doi: 10.1016/j.jconhyd.2014.12.001

Highly parameterized inversion of groundwater reactive transport for a complex field site

Luca Carniato[a], *Gerrit Schoups*[a], *Nick van De Giesen*[a], *Piet Seuntjens*[b,c,d], *Leen Bastiaens*[b] *and Hans Sapion*[e]

[*] Corresponding to the author phone: +31 (0)15 27 84025; Fax: +31 (0)15 27 85559; e-mail: l.carniato@tudelft.nl

[a]Department of Water Management, Delft University of Technology, PO Box 5048, 2600 GA Delft, Netherlands

[b]Flemish Institute for Technological Research (VITO), Boeretang 200, 2400 Mol, Belgium

[c]University of Ghent, Coupure Links 653, B-9000 Ghent, Belgium

[d]University of Antwerp, Groenenborgerlaan, 2000 Antwerp, Belgium

[e]SAPION, Oude Bevelsesteenweg 51, 2560 Nijlen, Belgium.

Abstract

In this study a numerical groundwater reactive transport model of a shallow groundwater aquifer contaminated with volatile organic compounds is developed. In addition to advective-dispersive transport, the model includes contaminant release from source areas, natural attenuation, abiotic degradation by a permeable reactive barrier at the site, and dilution by infiltrating rain. Aquifer heterogeneity is parameterized using pilot points for hydraulic conductivity, specific yield and groundwater recharge. A methodology is developed and applied to estimate the large number of parameters from the limited data at the field site (groundwater levels, groundwater concentrations of multiple chemical species, point-scale measurements of soil hydraulic conductivity, and lab-scale derived information on chemical and biochemical reactions). The proposed methodology relies on pilot point parameterization of hydraulic parameters and groundwater recharge, a regularization procedure to reconcile the large number of spatially distributed model parameters with the limited field data, a step-wise approach for integrating the different data sets into the model, and high performance computing.

The methodology was proven to be effective in reproducing multiple contaminant plumes and in reducing the prior parameter uncertainty of hydraulic conductivity and groundwater recharge. Our results further indicate that contaminant transport predictions are strongly affected by the choice of the groundwater recharge model and flow parameters should be identified using both head and concentration measurements.

Keywords: reactive transport; heterogeneity; pilot points; inverse modelling; groundwater recharge

1 Introduction

Subsurface reactive transport models are increasingly applied to real contaminant sites. However, major challenges are present when applying such models to reproduce the observed concentration measurements and attempt to use them as predictive tools. One of these challenges is the correct conceptualization and description of the subsurface processes using a limited amount of measurements (Gupta et al., 2012; Matott and Rabideau, 2008) and the computational burden. In practical terms, simulation of solute transport over a period of years to decades may require hours or days to complete on modern personal computers (Konikow, 2011). For these reasons and to avoid complexity not justified by the available data, simplifying assumptions are often made regarding the spatial distribution of aquifer parameters, groundwater flow and transport dynamics, degradation rates and parameter inference procedures (Hill, 2006).

In numerous studies homogeneous aquifer properties (within zones, layers or over the entire model domain) are used (D'Affonseca et al., 2011; Karlsen et al., 2012; Vandenbohede et al., 2013). Disadvantages of simple parameterization schemes are that the real response of the physical system might not be captured, introducing structural errors (Gallagher and Doherty, 2007) and hampering the ability to understand the natural system through model calibration (Hunt et al., 2007). Only a limited number of field-scale reactive transport studies directly inferred heterogeneity from available data (Fienen et al., 2009 (b); Tonkin and Doherty, 2009), whereas abundant literature is present for flow only problems (Hayley et al., 2014; Laloy et al., 2013; Yoon et al., 2013). Tonkin and Doherty (2005) applied the pilot point method (Marsily, 1984) to infer spatially variable flow and transport parameters (hydraulic conductivity, recharge and porosity) at the Hampton Bays Site, New York. In their approach a large number of model parameters were defined and the computational burden limited through the definition of "super parameters". The method was used to reproduce the observed MTBE (Methyl tert-butyl ether) concentrations at the site, effectively demonstrating that a better reproduction of the observations was obtained when aquifer

heterogeneity is accounted for. Kowalsky et al. (2012) studied the effect of different parameterizations of the hydraulic conductivity field (e.g. pilot point number and locations) in a synthetic tracer experiment, indicating the need for real applications where various data types are used in parameter inference. Fienen et al. (2009 (b)) used different data types (head, oxygen and tritium isotopic measurements) with a geostatistical method (Hoeksema and Kitanidis, 1984; Kitanidis and Vomvoris, 1983) to infer hydraulic conductivities of an isthmus comprised of two lakes in the Trout Lake watershed, northern Wisconsin, United States. They concluded that the flexible parameterization offered by the geostatistical method and the simultaneous use of multiple data sources improved the flow path delineation in the isthmus zone. In all cases, hundreds to thousands model parameters were used, combined with parameter regularization (Carrera et al., 2005; Yeh, 1986) to include prior parameter knowledge (Fienen et al., 2009 (a)). Pilot point and geostatistical methods allow the optimal level of complexity to be inferred directly from the data, provided that the model is correctly conceptualized and the correct assumptions about prior parameter knowledge are made.

Besides heterogeneity in hydraulic conductivity, spatial and temporal variation of groundwater recharge is important in modelling contaminant transport in shallow unconfined aquifers, due to the possible dilution effect by infiltrating rainwater. For example, Kowalsky et al. (2011) incorporated geochemical and time-lapse resistivity data in a hydrogeochemical model of the Oak Ridge Integrated Field Research Challenge (IFRC) site in Tennessee, United States. In their model it was assumed that groundwater recharge determines nitrate concentrations in the unconfined aquifer, in particular in the shallow part. Their study also points to the need for spatially extensive datasets (including chemical concentrations and geophysical measurements) to monitor recharge related concentration variations. Şengör and Ünlü (2013) developed a numerical model to determine the extension of acrylonitrile contamination at a spill site in Turkey. In their long term simulations (2001 to 2011), the size of the plume in a high permeability zone shrank significantly due to dilution by groundwater recharge. In these types of problems, flow and transport in the unsaturated

zone should ideally also be modelled, further increasing the computational demand (Yabusaki et al., 2011). A simpler approach is to assume groundwater recharge equal to the average net balance at the water table (D'Affonseca et al., 2011) or a spatially variable fraction of this balance (Hayley et al., 2014; Tonkin and Doherty, 2005). Assefa and Woodbury (2013) estimated groundwater recharge in the Okanagan basin (Canada) by calibrating a HYDRUS-1D model (Simunek et al., 2005) using soil moisture data, and extrapolating the results over the entire basin (245 km^2) based on soil characteristics. Their results show significant spatial variability in recharge, varying from 12 to 170 mm y^{-1}. On a larger scale (3600 km^2), Hayley et al. (2014) estimated groundwater recharge and horizontal hydraulic conductivity from head and flow data, also obtaining variable groundwater recharge rates.

Another important issue concerns the calibration methodology. In most of the reactive transport studies, flow parameters are calibrated first against head and flow data to provide the flow field to be used in reactive transport calculations (D'Affonseca et al., 2011; Gorelick et al., 1983; Prommer et al., 2009). Afterwards, the remaining reactive transport parameters are calibrated on concentration data, using independent estimations (e.g. lab experiments or field observations) and refining the initial guesses by manual calibration. The limitation of this approach is that the information about flow parameters contained in the concentration measurements is not used. Many synthetic and lab-scale studies demonstrate that concentration data are more informative of the local subsurface heterogeneity than groundwater head data (Pollock and Cirpka, 2012; Wagner, 1992).

In this study, we explicitly tackle the challenges discussed above, by means of an application of existing methodologies to a complex real-world contaminated site. Our study goes beyond existing applications which typically are restricted to single reactive species or synthetic aquifers. Applications of highly parameterized inversion of multi-component reactive transport models are not widely reported, and our study illustrates both the benefits and limitations of such an approach for real-world applications. Specifically, we show that parameter estimation in shallow heterogeneous contaminated aquifers strongly influenced by recharge dynamics is possible by a

combination of regularization, high-performance computing, and a step-wise approach of parameter refinement using laboratory and field data. The methodology is evaluated in terms of reproducing the observations, realism of the estimated parameters and reduction of the prior parameter uncertainty.

2. Methods

2.1 Study site

The studied contaminated site, depicted in Figure 1, is located in Wilrijk, just south of Antwerp, Belgium. The factory shown in the Figure 1 began production of compressors around 1951 and used chlorinated solvents mainly for painting and degreasing activities. The first use of chlorinated solvents (VOC) occurred in 1957, including tetrachloroethene (PCE), trichloroethene (TCE) and 1,1,1-trichloroethane (1,1,1-TCA or TCA), hereafter referred to as source contaminants. The use of VOC stopped in 1996, when it was banned by Flanders environmental law. Historically, the use of chlorinated solvents at the site has concentrated around three source locations and has resulted in contamination of the underlying aquifer, generating a contamination plume spreading from the factory to a pasture area next to the factory (Figure 1). The aquifer mainly consists of quaternary fine sand deposits, underlain by a low-permeable thick clay deposit ("Boom formation") at an average depth of 4.5 m below land surface (https://dov.vlaanderen.be). Groundwater flows laterally on top of the clay layer from factory to pasture, as shown in Figure 1 by contoured average groundwater levels (based on 731 measurements between 2001 and 2012).

In order to delineate the extent of the contamination and design a remediation strategy, contaminant concentrations, including source contaminants and their products (mainly cis-dichloroethene (cis-DCE) and vinyl chloride (VC)), were measured in 123 piezometers between 2000 and 2005. Most of the piezometers were screened one meter above the clay layer, since most of the contaminants were found at that depth.

In October 2005, a permeable reactive barrier was installed at the site (blue line in Figure 1). The barrier consists of two trenches, separated by an impermeable section, each approximately 95 meter long and 0.3 meters wide, penetrating the entire depth of the phreatic aquifer. The trenches were filled with a mixture of fine iron and sand (20% and 80% in volume, respectively). After barrier installation, monitoring of contaminant concentrations focused on areas near the barrier and in the pasture (Figure 1(b)). The following sections detail development of a groundwater flow and reactive transport model for the site, with the aim of quantitatively reconstructing historical contamination (starting in 1957), and predicting future plume development.

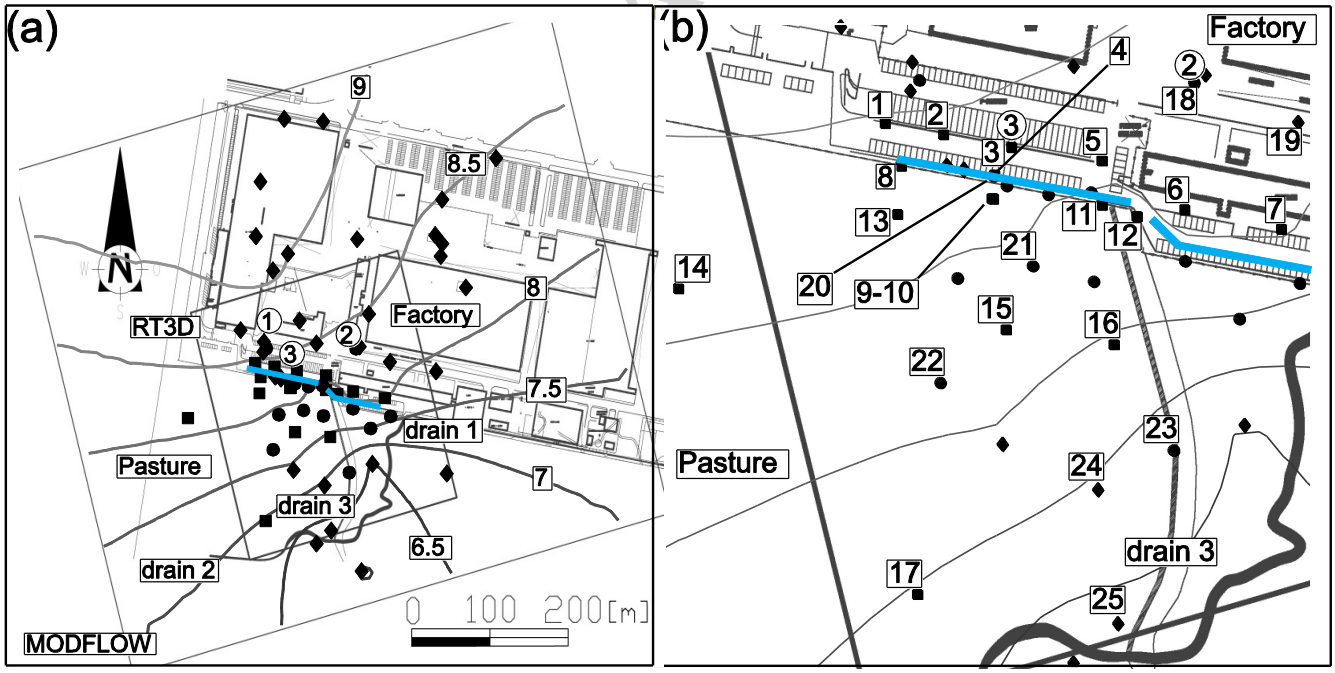

Figure 1. (a) Areal view of the site with labelled isophreatic levels and drain locations, flow (MODFLOW) and reactive transport domains (RT3D) and source locations (numbered circles). Diamonds correspond to piezometers where groundwater levels where monitored with bimonthly frequency in 2011, squares are piezometers where slug tests were performed, and dots are piezometers where concentrations were monitored with semiannual frequency in 2009-2011. The blue line indicates the permeable reactive barrier.

2.2 Flow model

A conceptual picture of relevant flow and transport processes at the site is shown in Figure 2. Groundwater flow was described with the 3-D groundwater flow equation:

$$\frac{\partial}{\partial x}\left(K_{xx}\frac{\partial h}{\partial x}\right)+\frac{\partial}{\partial y}\left(K_{yy}\frac{\partial h}{\partial y}\right)+\frac{\partial}{\partial z}\left(K_{zz}\frac{\partial h}{\partial z}\right)+W=S_s\frac{\partial h}{\partial t} \quad (1)$$

where K_{xx}, K_{yy} and K_{zz} are the saturated hydraulic conductivity values in x, y, and z directions (m d^{-1}); h is the total hydraulic head (m); W is the source/sink term representing recharge and evaporation (d^{-1}) and S_s is the specific storage (m^{-1}) for confined aquifers. In unconfined aquifers Equation (1) is integrated over the vertical direction and the specific storage is replaced by the aquifer specific yield S_y (-). Groundwater flow was simulated using MODFLOW-2000 (Harbaugh et al., 2000), within the domain indicated in Figure 1(a). The model is oriented along the main flow direction and is composed of 2 layers, 133 rows and 125 columns.

Land surface elevation was reconstructed by kriging measured elevations at 62 piezometers. Clay depths were obtained by subtracting the estimated thickness of the aquifer at 148 piezometers from the kriged land surface elevation. The bottom model layer coincides with the screened interval of the piezometers. The top layer was modelled using the convertible option of MODFLOW 2000, where the layer is model as unconfined if the water table does not exceed the elevation of the land surface and confined otherwise. The bottom layer was modelled as confined, since observed groundwater levels never drop below the top of the layer. This approach produced almost identical results of treating both layers as convertible but avoided the drying and re-wetting for some cells (which might cause the simulation failure).

General head boundary conditions (Harbaugh et al., 2000) were used at the north (upstream) and south (downstream) sides of the model domain, while no-flow boundary conditions were specified for the west and east boundaries. Three drains were included in the pasture area of the model, as observed in the field (Figure 1 (a)). No flow was assumed to occur below the bottom layer, due to presence of the low permeable clay (Boom clay formation). Special attention was paid to modelling

aquifer heterogeneity and spatial variations in recharge entering the aquifer in the pasture area, as discussed in the following two subsections.

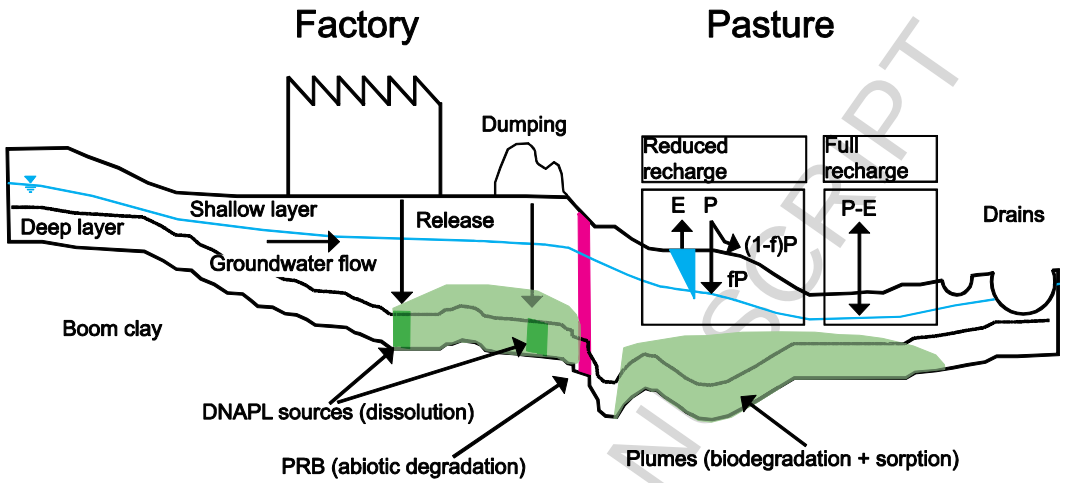

Figure 2. Conceptual model of the flow and reactive transport processes at the site.

2.2.1 Aquifer properties heterogeneity

Spatial variation in hydraulic conductivity, specific yield and recharge was modelled using the pilot point method (Certes and de Marsily, 1991; RamaRao et al., 1995). In the pilot point method, the unknown parameters are estimated for a set of points collocated within the domain. The corresponding spatially distributed parameter field is obtained through kriging the pilot points values over the model domain. As shown in Figure 3(a), specific yield pilot points were placed on a regular grid (22.5 m apart near the barrier and further apart in areas with fewer groundwater and concentration measurements), resulting in 127 pilot points. Infiltration fraction pilot points were placed only in the permeable pasture area where measurements were collected (in Figure 3(b)), resulting in 43 pilot points.

It was assumed that the aquifer is horizontally isotropic ($K_{xx} = K_{yy}$ = HK, horizontal hydraulic conductivity) but vertically anisotropic. Horizontal hydraulic conductivity parameterization was similar to the one used for specific yield (Figure 3(c)), with a local refinement along the main plume direction (Figure 3(d)), yielding 178 pilot points. Spatial correlation of the heterogeneous aquifer

properties were assumed to be described by an exponential variogram. A variogram range of 150 m was adopted for specific yield and hydraulic conductivity fields and 105 m for infiltration fraction pilot points, corresponding to the maximum pilot point to grid cell distance (Doherty et al., 2010). The variogram range was kept fixed in the inversion tests as the inversion results are expected to be more influenced by locations and number of pilot points used in the inversion (Kowalsky et al., 2012). The sill for log-transformed specific yield was estimated as 0.137, which corresponds to ¼ of the variation range squared, assuming values for specific yield from 0.01 to 0.3 (Johnson, 1963) and a log normal distribution of the specific yields values. Similarly, the sill for log-transformed infiltration fractions was estimated at 0.063 (assuming a variation range for recharge from 0.1 to 1). The sill for log-transformed horizontal hydraulic conductivity was estimated as 0.254, based on the variance of values for log-transformed hydraulic conductivity determined from slug tests (Figure 7). Finally, in the absence of direct measurements, vertical hydraulic conductivity was assumed to be 10 times smaller than the corresponding horizontal hydraulic conductivity (Todd, 1959). Furthermore, vertical variation in aquifer properties was neglected, and thus the same values were adopted for both model layers. This latter assumption is supported by slug test data from piezometers 9 and 10, which are screened in the deep and shallow layer respectively (Figure 8).

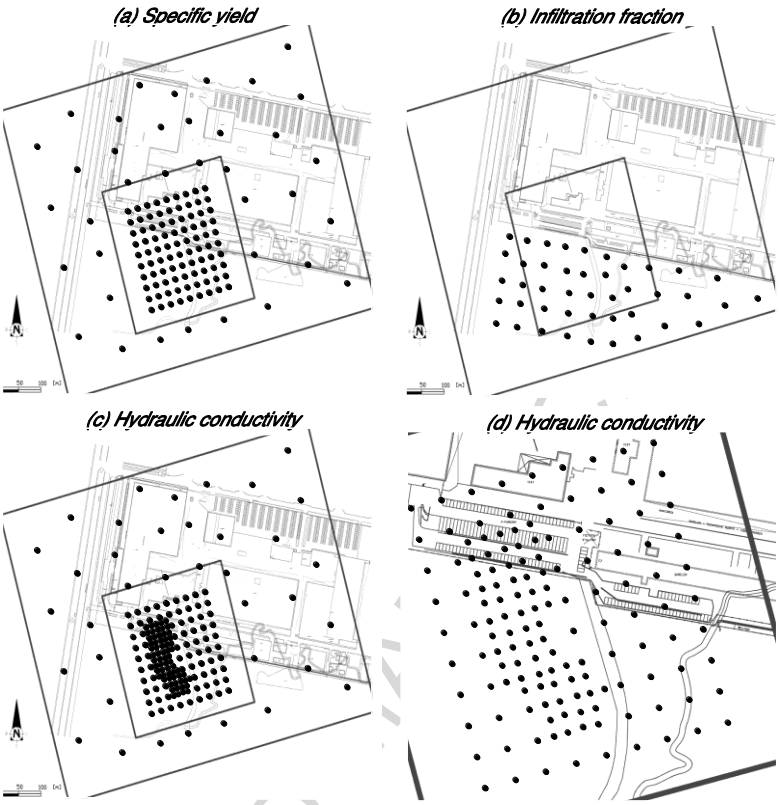

Figure 3. Pilot points for (a) specific yield, (b) infiltration fraction, and (c) hydraulic conductivity. In Figure (d) the pilot point refinement along the main plume direction for hydraulic conductivity is shown.

2.2.2 Recharge

The pasture area of the shallow unconfined aquifer exhibits dynamic variations in groundwater levels caused by the complex interplay between precipitation, infiltration, runoff, evaporation, and recharge. To quantify recharge and/or evaporation from the, mostly shallow, water tables at the site, two different models were considered.

In the first model, referred to as the "full recharge model", net "recharge" (positive or negative) to/from the water table was estimated as the difference between weekly precipitation and potential evaporation data from a nearby meteorological station (Westdorpe, Netherlands). In this model, runoff was assumed to occur when the water table reaches the land surface, implemented here with the MODFLOW drain package by specifying virtual drains at the land surface with a large

conductance value. The full recharge model might be justified by the shallow depth of the water table (in most circumstances measured to be no lower than 1.5 meters from the ground surface), but might introduce too much water in the aquifer which can be drained out from the system only by high hydraulic conductivity values.

In the second recharge model, referred to as the "reduced recharge model", infiltration was first estimated as a (temporally constant, but spatially variable) fraction of precipitation, with the remaining water assumed to be lost as runoff. Infiltrated water was then added as recharge to the water table, from where it can be lost again by evaporation. Hence, recharge and evaporation were treated separately, and were implemented using the MODFLOW recharge and evapotranspiration packages, respectively. The rate of evaporation from the groundwater table was assumed to vary linearly as a function of water table depth, with a maximum equal to potential evaporation for water table at the land surface and zero for water table more than 2 meters below land surface (this extinction depth was estimated from an empirical equation reported in Shah et al. (2007)). The fraction of infiltrating precipitation was assumed to be spatially variable and parameterized with pilot points (Figure 3(b)). Temporal variation in infiltrating fractions was not taken into account.

2.3 Reactive transport model

Three-dimensional advective-dispersive reactive transport was simulated using the RT3D code (Clement, 1997) for an aerial extent contained within the larger flow model domain, as shown in Figure 1(a). Transport was simulated with the standard advective-dispersive-reaction equation:

$$\frac{\partial C_k}{\partial t} = \frac{\partial}{\partial x_i}\left(D_{ij} \frac{\partial C_k}{\partial x_j} \right) - \frac{\partial}{\partial x_i}\left(v_{eff,i} C_k \right) + \frac{W}{por} C_{Wk} + r_k \quad k = 1, \ldots, m_c \tag{2}$$

$$\frac{d\tilde{C}_k}{dt} = \tilde{r}_k \quad k = 1, \ldots, (n_c - m_c) \tag{3}$$

where i and j represent the spatial direction (x, y or z) and indexes repetition implies summation, n_c is the total number of species, m_c is the total number of aqueous-phase (mobile) species (thus, m_c

minus n_c is the total number of immobile species), C_k is the aqueous-phase concentration of the k^{th} specie (mol L^{-1}), $\tilde{C}_k$ is the solid-phase concentration of the k^{th} chemical specie (mol L^{-1}), D_{ij} is the hydrodynamic dispersion coefficient (m^2 d^{-1}), *por* is the effective porosity, v_{eff} is the effective velocity (m d^{-1}), C_{Wk} is the concentration of source/sink (mol L^{-1}), r_k represents the rate of all reactions occurring in the aqueous-phase (mol L^{-1} d^{-1}) and $\tilde{r}_k$ represents the rate of all reactions occurring in the soil-phase (mol L^{-1} d^{-1}). The coefficients D_{ij} of the dispersion matrix were calculated from longitudinal, horizontal transverse and vertical transverse dispersivities values (Burnett and Frind, 1987). The reaction term r_k, which accounts for depletion or production of contaminant *k*, can be expressed as:

$$r_k = \sum_i^{N_s} r_{k-SOU,i} - r_{k-DEG} + \sum_i^{p} r_{i-DEG} - r_{k-PRB} \tag{4}$$

where $r_{k\text{-}SOU,i}$ is the release rate of the compound *k* from the source *i* (1, 2 or 3, as shown in Figure 1(a)), $r_{k\text{-}DEG}$ is the biodegradation rate of compound *k*, *p* is the number of compounds that degrades to *k* (Figure 4) and $r_{k\text{-}PRB}$ is the removal rate of *k* into the PRB. An example for TCE is reported below:

$$r_{TCE} = r_{TCE-SOU,1} + r_{TCE-SOU,3} - r_{TCE-DEG} + r_{PCE-DEG} - r_{TCE-PRB} \tag{5}$$

where contaminant degradation by zero-valent iron was assumed to mainly occur by β-elimination and much less by hydrogenolysis (Arnold and Roberts, 2000), with no formation of intermediates. In the following sections, each chemical and physical process included in the model is discussed in more detail.

2.3.1 Contaminant dissolution from the source areas

Source contaminants (PCE, TCE and TCA) are known to form dense non aqueous phase liquid phases (DNAPL), which tend to migrate downwards due to the gravity force and slowly dilute in groundwater. In this study it was assumed that pure phase contaminants were released on the ground surface and have migrated and accumulated in the bottom layer (Figure 2). The pure phase

DNAPL pools in the bottom layer dilute in groundwater forming the observed contaminant plumes. Hence, the change in time of DNAPL phase mass for each parent compound was described by the following expression:

$$\tilde{r}_{k-SOU,i} = \min\left[-k_{la}(C_{k,i}^{*} - C_k), 0\right] + k_{k-SOU,i} \quad (6)$$

where k_{la} is a mass transfer coefficient, $C_{k,i}^{*}$ represents the equilibrium solubility in groundwater for parent contaminant k (TCA, PCE or TCE) at the specific source location i, C_k is the contaminant concentration in groundwater and $k_{k\text{-}SOU,i}$ is the release rate of the parent contaminant k during the 1957-1996 period at source location i (mol L^{-1} d^{-1}). The equilibrium contaminant solubility of each parent contaminant was modelled by Raoult's law (Schwarzenbach et al., 2005):

$$C_k^{*} = C_{k-SOL}\gamma_k \frac{\tilde{C}_k}{\sum_{i=1}^{N_p}\tilde{C}_{k,i}} \quad (7)$$

where $C_{k\text{-}SOL}$ is the solubility of compound k in groundwater (Pankow and Cherry, 1996), γ_k the activity coefficient (assumed to be unity) and N_p is the number of source contaminants in the specific source area. Based on concentration measurements, sources 1 and 3 were assumed to contain PCE and TCE, whereas source 2 only TCA. In none of the piezometers pure phase DNAPL was detected, justifying the hypothesis that the DNAPL phase in the source areas is small and does not influence water phase permeability. For the mobile domain, the release from the sources is equal to the first part of equation (6), but with opposite sign:

$$r_{k-SOU,i} = \max\left[k_{la}(C_{k,i}^{*} - C_k), 0\right] \quad (8)$$

2.3.2 Biodegradation of contaminants

Following Johnson and Truex (2006), the degradation of source contaminants (PCE, TCE and TCA) was modelled as a sequence of irreversible kinetic degradation reactions (Figure 4). The network does not include trans-DCE, 1,1,2-TCA and 1,2-DCA (1,2-Dichloroethane) contaminants, as these were measured at low concentrations. The biodegradation reactions were assumed to occur

under anaerobic conditions with production of intermediate contaminants (TCE, cis-DCE, VC and DCA (1,1-Dichloroethane)). In Figure 4, the solid arrows indicate reductive dechlorination reactions, where contaminants are used as electron acceptors by micro-organisms. The electron donor in these reactions is usually hydrogen gas, produced by fermentation of an organic substrate (Distefano et al., 1992; He et al., 2002). As such, dechlorination both affects and depends on the availability of fermentable substrate, with low degradation rates and substrate levels in the interior of the contamination plume, and high degradation rates and substrate levels at the fringes of the plume, where the plume is in contact with pristine aquifer material. A similar pattern was observed at the site: laboratory biodegradation batch experiments using sampled groundwater and aquifer material from piezometers located within the plume (piezometers 9, 10, 21 and 16) revealed low organic carbon content (< 0.3%) and no substantial degradation of contaminants for the duration of the experiments (384 days). On the other hand, piezometer 23, located at the fringe of the plume, showed high organic carbon content (5.4%) and significant contaminant biodegradation in the laboratory.

The interplay between degradation rates and substrate levels was accounted for by specifying rate expressions for the biodegradation processes in Figure 4 that depend on substrate concentration. For PCE, TCE, cis-DCE and VC, the degradation rate was modelled as:

$$r_{k-DEG} = S\mu_k \frac{C_k}{C_k + K_{hk}(1+\frac{C_{i,k}}{K_{hi}})} \quad (9)$$

where S is substrate concentration ($mol_S\ L^{-1}$), μ_k (mol mol_S^{-1} d^{-1}) and K_{hk} (mol L^{-1}) are the degradation rate coefficient and half-saturation constant for contaminant k, and $C_{i,k}$ is the concentration of the inhibitor i for compound k (e.g. TCE for PCE) with half-saturation constant K_{hi}. Compared to a simpler first-order approach, the introduction of inhibition at high $C_{i,k}$ concentrations accounts for the competition of electron acceptors for the available substrate and resulted in a separation of the different contaminant plumes, as observed at the site. The rate model

reported in Equation (9) resembles the one proposed by other studies (Clapp et al., 2004; Manoli et al., 2012; Rittmann and McCarty, 2001), although the hydrogen term was substituted with the substrate concentration, assuming the amount of dissolved hydrogen in groundwater directly proportional to the substrate content (substrate fermentation was not modelled).

For the biodegradation of TCA to DCA and DCA to ethane, a simpler first-order, substrate-dependent rate equation was used:

$$r_{k-DEG} = S\mu_k C_k \tag{10}$$

The degradation of TCA to DCE, indicated by the dashed arrow in Figure 3, occurs via dehydrochlorination, whereby one chloride atom and one proton are eliminated. As this is an abiotic reaction, its rate equation was assumed to be independent of substrate concentration S,

$$r_{TCA-DCE-DEG} = \mu_{TCA-DCE} TCA \tag{11}$$

with the rate coefficient $\mu_{TCA\text{-}DCE}$ estimated from measured in-situ groundwater concentrations (Table 1). Finally, consumption of fermentable substrate was considered proportional to the sum of all six biodegradation rates (solid lines in Figure 4):

$$\tilde{r}_S = -f_{S/VOC} \sum_{i=1}^{N_{bio}} r_{i-DEG} \tag{12}$$

where $f_{s/VOC}$ is a stoichiometric coefficient expressing the amount of substrate required for the degradation of one mole of contaminant. Its value depends on site-specific substrate composition and was estimated from measured in-situ groundwater concentrations (Table 1). In equations (9) to (12), substrate consumption by other electron acceptors (such as sulphate or carbon dioxide) was not explicitly modelled and biomass growth neglected. The assumption of constant biomass was also used in previous field-scale modelling studies (Clement et al., 2000; Rotter et al., 2011). The initial substrate concentration was estimated from the carbon content measured in uncontaminated piezometers (1.5% and 0.3% for a shallow and a deep piezometer, respectively), assuming $C_2H_7O_2N$ as representative molecule of the substrate.

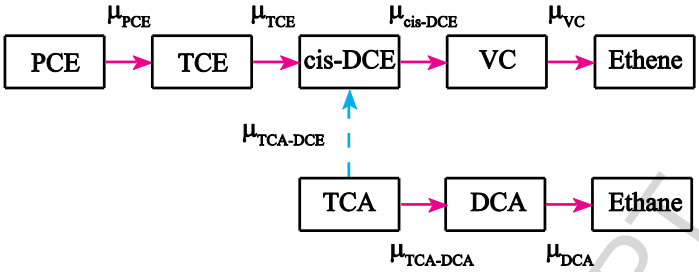

Figure 4. Biodegradation network. Solid arrows indicate reductive dechlorination (biotic) and the dashed arrow dehydrochlorination (abiotic).

2.3.3 Abiotic contaminant degradation within the reactive barrier

As groundwater flows through the permeable reactive barrier, dissolved contaminants come in contact with the reactive material (zero-valent iron), and are converted to non-toxic substances (such as ethene) via chemical (abiotic) reduction. Individual kinetic rates of abiotic contaminant degradation in the barrier were described by a mixed-order rate law (Wüst et al., 1999):

$$r_{k-PRB} = -k_{k-PRB} S_r \frac{C_k}{K_{kh-PRB} + C_k} \tag{13}$$

where $k_{k\text{-}PRB}$ is the rate coefficient per unit of iron reactive surface area (mol m^{-2} s^{-1}) for contaminant C_k, S_r is iron reactive surface area per unit water volume (m^2 L^{-1}), and $K_{kh\text{-}PRB}$ is the half-saturation constant (mol L^{-1}). As shown in Figure 1, the barrier is not oriented perpendicularly to the model domain: in the model it is represented as a series of reactive connected 2.5 m by 2.5 m grid cells, resulting in a staircase representation of the 0.3 m wide barrier.

Whereas in principle mineral precipitation within the barrier may decrease its reactivity over time, this was not accounted for in the current model, an assumption supported by reactivity tests performed in 2012 on reactive zero-valent iron material extracted from the in-situ barrier after 7 years of operation.

2.3.4 Contaminant sorption to aquifer material

Sorption was modelled as a reversible equilibrium process assuming a linear isotherm. The distribution coefficients $K_{d\text{-}k}$ (L kg^{-1}) were calculated as:

$$K_{d-k} = K_{oc-k} f_{oc} \tag{14}$$

where $K_{oc\text{-}k}$ is the contaminant specific partition coefficient (L kg^{-1}, (Wiedemeier et al., 2007)) and f_{oc} the carbon content measured in soil samples from the site (1.5% for the shallow layer and 0.3% for the deep one). The retardation factor R_k under equilibrium conditions was calculated as:

$$R_k = 1 + \frac{\rho_b}{por} K_{d-k} \tag{15}$$

here, ρ_b is the dry bulk density, set equal to 1628 kg L^{-1} (determined from angled core samples) and *por* is the effective porosity.

3 Calibration procedure

Several model parameters, listed in Table 1, were not directly measured in situ and were instead estimated from available groundwater level and concentration data. For this purpose, the model was set up to reproduce historical contamination at the site, starting from a clean aquifer. Hence, the simulations were started in 1957, the time of first use of chlorinated solvents at the site, and run until 2011, with most piezometer data available for the period 2001-2011. The aquifer was assumed to be initially free of contaminants. Calibration was then formulated as an optimization, or inverse problem, which consisted of finding parameter values that minimize discrepancies between measured and simulated groundwater levels and concentrations. Three different optimization problems were set up, each with its own objective function, data, and set of parameters to be estimated:

1. Optimization of flow parameters (step 1)

$$\Phi = \Phi_{m,1} + \beta^2 \Phi_r \tag{16}$$

2. Optimization of reactive transport parameters (step 2)

$$\Phi = \sum_{j=2}^{7} \Phi_{m,j} \tag{17}$$

3. Optimization of flow and reactive transport parameters (step 3)

$$\Phi = \sum_{j=1}^{7} \Phi_{m,j} + \beta^2 \Phi_r \tag{18}$$

where $\Phi_{m,j}$ is the measurement objective functions for the set j (weighted sum of the squared residuals), j is the measurement set index (j = 1 groundwater heads, j = 2 PCE, j = 3 TCE, j = 4 cis-DCE, j = 5 VC, j = 6 TCA, j = 7 DCA), β^2 is the regularization weight factor and Φ_r is the "regularization objective function", which incorporates the weighted squared differences between adjacent parameter values (smoothness regularization) and/or the differences of the parameters respect a specified value (preferred value regularization). When many parameters are estimated regularization is necessary to stabilize the inverse problem, otherwise unrealistic parameter estimations might be obtained (Doherty, 2003). For hydraulic conductivity a preferred value of 0.195 m d^{-1} was specified, equal to the mean hydraulic conductivity value estimated from the slug in and slug out tests (Figure 7). The preferred value for specific yield was specified at 0.1, which is a reasonable value for a sandy clay soil (Johnson, 1963). A smoothness regularization constraint was imposed for the recharge pilot points, with squared weights inversely proportional to the values of the variogram model. Besides parameter regularization, singular value decomposition with a truncation threshold of 1e-6 was used to improve numerical stability.

Figure 5 summarizes the method applied to estimate the model parameters. Before starting the optimizations plausible parameter values were estimated, based on the available lab and field measurements and literature studies. Afterwards, flow parameters were calibrated on the 420 transient groundwater head levels collect in 2011 (diamonds in Figure 1), whereas the pre 2011 measurements were used as validation dataset. In the optimization of reactive transport parameters (step 2), 18 parameters were calibrated on 2240 concentration data (corresponding to degradation, source and transport parameters in Table 1), keeping the flow field fixed as estimated from step 1.

In the optimization of flow and reactive transport parameters (step 3), all parameters were estimated from all measurements (420 head and 2240 concentration measurements), starting from the flow field obtained in step 1 and the initial reactive transport parameters. Therefore, two optimal parameter vectors (369 parameters) were compared. The first obtained after step 2, with flow parameters inferred from head measurements and transport and chemical parameters inferred from concentration measurements. The second obtained after step 3, refining the estimations of hydraulic conductivities and drain conductances obtained at step 1 with concentration data and determining reactive transport parameters from head and concentration measurements.

Minimization of the objective functions (16)-(18) was performed using BeoPEST (Hunt et al., 2010), a particular version of PEST (Doherty, 2007) software package which allows an efficient parallelization of the model runs. In objective function (16) the weight of the regularization constrains is determined by β^2, which is calculated at the starting of each Levenberg-Marquardt iteration to ensure that $\Phi_{m,1}$ rises no higher than a user specified target objective function $\Phi^l_{m,1}$ (Doherty and Skahill, 2006). Therefore, $\Phi^l_{m,1}$ has a strong influence on the estimated parameter fields, and should not be specified below the expected measurement and model errors. For step 1 $\Phi^l_{m,1}$ was set to 9.45, which corresponded to a RMSE of 0.15 m. Such value was deemed reasonable and accounts for the precision of the measurements and daily groundwater fluctuations not reproduced by the model. Flow inversions were performed with the full and reduced recharge models. In order to determine the appropriate recharge model, conservative transport simulations were performed with the flow fields estimated from both recharge models. In these tests neither sorption nor biodegradation were included, thus simulating the maximum spreading of the contamination and the dilution effect by rainwater. After choosing the most appropriate recharge model, multicomponent reactive transport model was simulated, activating all chemical processes described above.

In Equation (18) head and concentration measurements were used to calibrate flow and transport parameters simultaneously imposing regularization with different measurement sets. As for the flow optimization (Equation (16)), single measurement objective function targets $\Phi^{l}_{m,j}$ can be specified for each set, based on the expected level of misfit due to the measurement and model errors. In this case, the weights assigned to the residuals (observed minus simulated values) were adjusted during the optimization using the following equation (Doherty, 2007):

$$w^{2}_{IT,ij} = w^{2}_{IT-1,ij} \frac{\Phi_{mIT,j}}{\Phi^{l}_{m,j}} \tag{19}$$

where $w_{IT,ij}$ is the weight assigned to the residual i of the set j at the iteration IT and $\Phi_{mIT,j}$ is the measurement objective function of the set j at the iteration IT (calculated with the initial weights). Therefore, the weights are increased if the current measurement objective function of the set j is above $\Phi^{l}_{m,j}$ and decreased otherwise.

In absence of model errors, initial weights should be assigned inversely proportional to the measurement error, usually assumed equal to the measured concentration multiplied by a coefficient of variation (Hill and Tiedeman, 2007; Hill et al., 2013). Using this approach in step 2 resulted in an underestimation of the simulated concentrations over the entire model domain due to an overestimation of the weights for small concentration values. In our study residuals were also generated by model errors with unknown variance. Using the approach of Sun (1994) an initial estimation of the total residual variance (measurement plus model error) can be obtained from the residuals at the initial parameter value, by dividing the sum of the residuals belonging to each measurement set j by the number of measurements n_j contained in that set. Using these weights, the initial contribution of each measurement set to the objective function is equal to n_j, resulting in a better reproduction of the measured concentrations in step 2 and 3. In step 1, $w_{0,1}$ was set equal to 1 for all groundwater level measurements.

Posterior parameter uncertainty was assessed using PREDUNC7 utility of the PEST software suite, where a linear relation between measurements and model parameters is assumed. The utility

requires an estimation of the prior parameter covariance matrix, estimated from the variograms for pilot point parameters and from plausible variation intervals for other parameters. Two posterior covariances of model parameters were estimated with PREDUNC7 utilities at the two optimal parameter vectors. The posterior parameter standard deviations were then compared to assess the reduction of prior parameter uncertainty when assimilating head and concentration simultaneously (step 3) against the separate assimilation of head and concentrations (step 1 and 2).

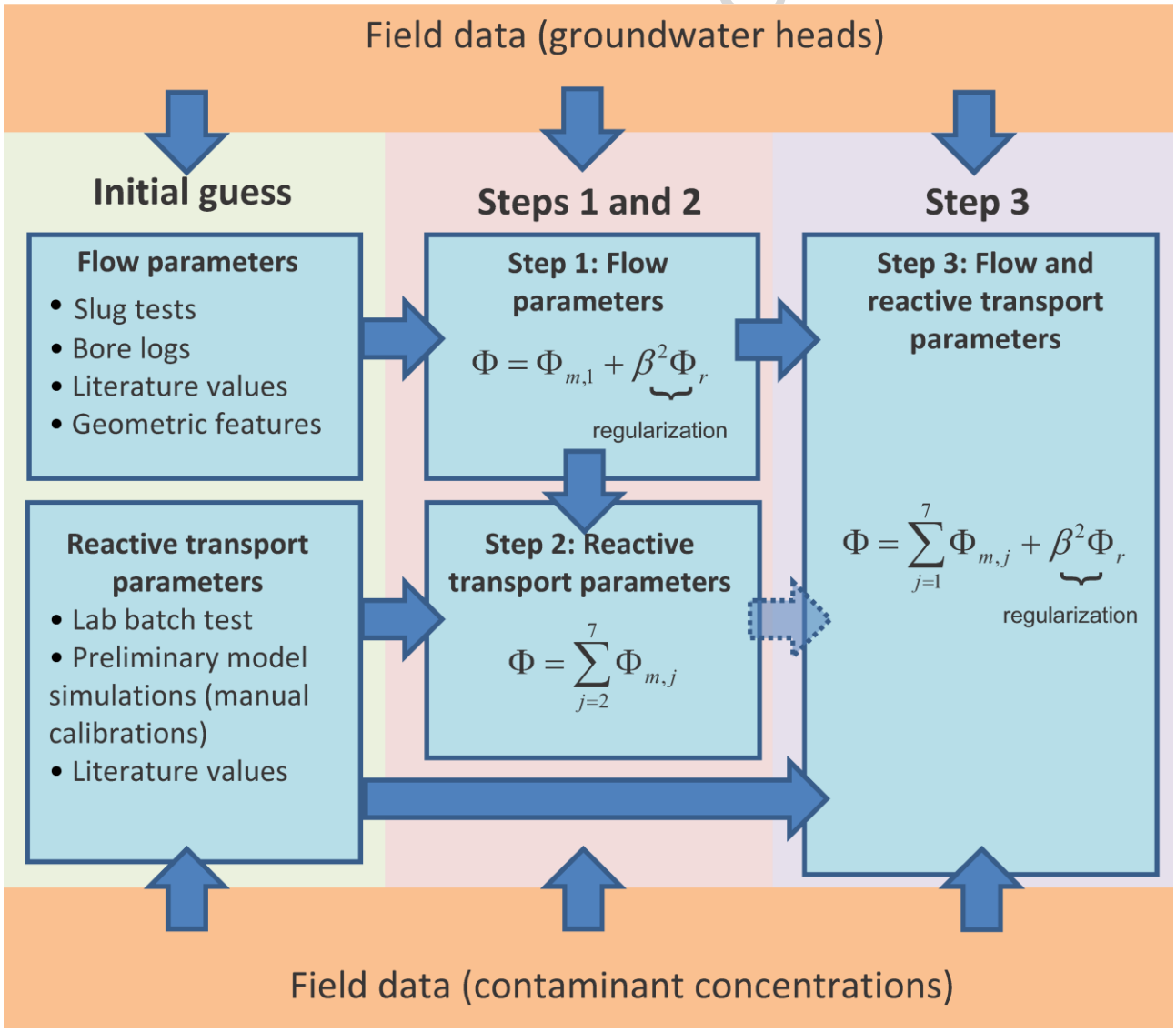

Figure 5. Step-wise approach of parameter refinement.

4 Results

The results are organized as shown in figure 5. First, we motivate the initial parameter guesses in section 4.1.Then the results of the flow parameters optimization (step 1) and conservative transport simulations for the selection of the appropriate recharge model are presented in section 4.2. Section 4.3 presents the results of step 2 and section 4.4 the results of step 3. Results are evaluated in terms of realism, model fit to available measurements, and reduction of prior parameter uncertainty.

4.1 Initial parameter estimates from lab data and literature

Initial estimates of the model parameters must be provided before starting any gradient based optimization procedure. In principle these estimates should be obtained from separate measurements (e.g. slug test measurements for hydraulic conductivity). In absence of direct measurements appropriate initial values from literature studies can also be used.

The initial parameter estimates are reported in Table 1. The average hydraulic conductivity estimated from slug tests (Figure 8) was used as initial value for hydraulic conductivity pilot points. For specific yield pilot points an initial value of 0.1 was assumed, as supported by literature data for the soil type analyzed in the bore logs. The initial recharge fraction for the reduced recharge model was assumed equal to 1. The conductances of the three drains (Figure 1) were estimated from in situ topographic measurements.

The degradation rate coefficients μ_k (Equation 9) for PCE, TCE, cis-DCE and VC were initially derived from lab batch tests. However, using these degradation rates the concentrations were underestimated over the entire model domain even at elevated k_{la} values (Equation (8)). Such underestimation can negatively affect the performance of the gradient based optimization algorithms because the sensitivity of the measurements with respect of model parameters becomes zero. Therefore, a set of preliminary model simulations were performed to adjust the rate coefficients and obtain a realistic configuration of the multiple contaminant plumes. For μ_{TCA}, μ_{TCA}-

$_{DCE,}$ μ_{TCA} and $f_{s/VOC}$ separate lab measurements were not available and their initial values were derived from literature studies. The half-saturation constants K_{hk} in Equation 9 were estimated from the study of Haston and McCarty (1998).

The contaminant degradation parameters of the PRB ($k_{k\text{-}PRB}$, S_r and $k_{kh\text{-}PRB}$ in Equation (13)) were determined from a column flow-through experiment performed with the same groundwater and reactive media of the PRB installed at the site, as described in detail in Carniato et al. (2012). To account for the coarse barrier discretization in the model, the barrier degradation rate coefficients $k_{k\text{-}PRB}$ determined from the column experiment were divided by 8.3, the ratio of the block size (2.5 m) and the effective barrier thickness (0.3 m).

Since no quantitative information was available about contaminant disposal and release rates through time, $k_{k\text{-}SOU,i}$ for each parent compound and source area were estimated from preliminary model simulations, together with the mass transfer coefficient k_{la}. The lowest estimation of the total released mass (not accounting for biodegradation and dilution processes) was obtained integrating the total contaminant concentration over the entire aquifer volume. The results of this integration yield a contaminant mass of 22 kg, far below the one obtained integrating the initial release rates over the spillage period.

The initial effective porosity was estimated from literature data. The longitudinal dispersivity was estimated from preliminary model simulations whereas the horizontal transverse and vertical transverse dispersivities were fixed at 0.1 and 0.01 times the longitudinal dispersivity respectively (Zheng and Wang, 1999).

Table 1. Initial model parameters estimates (HK = horizontal hydraulic conductivity, SY = specific yield, DSP = longitudinal dispersivity, TRPT = horizontal transverse to longitudinal dispersivity ratio, TRPV = vertical transverse to longitudinal dispersivity ratio)

Parameters	Initial guess	Notes
Flow parameters		
HK ($m\ d^{-1}$)	0.194	Average value from all slug tests
SY (-)	0.1	Plausible value for sandy clay soils (Johnson, 1963)
Recharge fraction (-)	1	Initially, it is assumed that all precipitation infiltrates
Conductance drain 1, 2 and 3 ($m\ d^{-1}$)	70, 70, 10	$=W/(K*d)$, where drain widths W are estimated as 7, 7 and 1 m respectively, drain beds d are assumed to be 0.1 m thick, with hydraulic conductivities K equal to 1 $m\ d^{-1}$
Degradation coefficients[(a)]		
μ_{PCE} ($mol\ mol_S^{-1}\ d^{-1}$)	1.80e-8	Using lab degradation coefficient (7.3e-8), high TCE concentrations were simulated at the sources, even at low contaminant release rates
μ_{TCE} ($mol\ mol_S^{-1}\ d^{-1}$)	1.00e-7	Using lab degradation coefficient (1.89e-5), no TCE contamination was simulated in the pasture area
μ_{DCE} ($mol\ mol_S^{-1}\ d^{-1}$)	3.00e-9	Using lab degradation coefficient (4.34e-6), no DCE contamination was simulated in the pasture area
μ_{VC} ($mol\ mol_S^{-1}\ d^{-1}$)	1.71e-9	Using lab degradation coefficient (9.55e-7), no VC contamination was simulated in the pasture area
$\mu_{TCA\text{-}DCA}$ ($mol\ mol_S^{-1}\ d^{-1}$)	6.14e-1	Obtained by dividing the maximum dechlorination rate coefficient of Suarez and Rifai (1999) by the estimated substrate content
$\mu_{TCA\text{-}DCE}$ (d^{-1})	1.70e-3	Maximum dehydrochlorination rate coefficient reported in Suarez and Rifai (1999)
μ_{DCA} ($mol\ mol_S^{-1}\ d^{-1}$)	5.41e-3	Based on the value reported in Suarez and Rifai (1999) divided by the estimated substrate content
$f_{S/VOC}$(-)	600	One mole of organic substrate (in the form of $C_2H_7O_2N$) can yield up to 20 electron equivalents when it is completely oxidized to CO_2 (10 H_2 equivalents). Existing field data indicate that only 0.01% to 0.1% of this potential is available to dechlorinating bacteria. Therefore, between 100 to 1000 mol of $C_2H_7O_2N$ are required to remove one chloride atom from one mole of contaminant (e.g. going from PCE to TCE). Bauer et al. (2006) measured electron donating capacities between 0.07 and 1.5 milliequivalents per gram of carbon for dissolved organic matter (DOM) in a peat bog. Using their estimates and assuming $C_2H_7O_2N$ to be representative of the in-situ substrate, 22 to 476 moles are necessary to remove one chloride atom from one mole of chlorinated contaminant
Source parameters		
k_{la} (d^{-1})	1e-4	Higher mass transfer coefficients caused solver failure at low release rates (fast mass transfer)
$k_{PCE\text{-}SOU,1}$ ($mol\ L^{-1}\ d^{-1}$)	1e-6	Manual calibration (11.05)[(b)]
$k_{TCE\text{-}SOU,1}$ ($mol\ L^{-1}\ d^{-1}$)	3e-6	Manual calibration (26.26)
$k_{TCA\text{-}SOU,2}$ ($mol\ L^{-1}\ d^{-1}$)	4e-5	Manual calibration (355.48)

$k_{PCE\text{-}SOU,3}$ (mol L^{-1} d^{-1})	1e-7	Manual calibration (1.10)
$k_{PCE\text{-}SOU,3}$ (mol L^{-1} d^{-1})	1e-7	Manual calibration (0.88)
Transport parameters		
DSP (m)	5	Manual calibration
TRPT (-)	0.1	Value suggested by Zheng and Wang (1999)
TRPV (-)	0.01	Value suggested by Zheng and Wang (1999)
por (-)	0.1	Plausible value for sandy clay soils (McWhorter and Sunada, 1977)
Number of parameters	369	

(a) degradation parameters were estimated only for the batch experiment performed with piezometer 23 soil and groundwater, for other piezometers biodegradation was negligible. Suarez and Rifai (1999) reported that degradation rates in lab conditions are higher than field conditions, with difference between 1 to 2 orders of magnitude. (b) In brackets the total released mass for each source is reported. Integration of the total contaminant concentration in the aquifer volume yield a mass of about 22 kg (assuming a total porosity of 0.4), to be considered the lowest estimate of the total released contaminant mass (not accounting for biodegradation and dilution processes).

4.2 Step 1: refinement of flow parameters

In Figure 6, horizontal hydraulic conductivities and specific yield values estimated with the full recharge model (figures 6(a) and 6(b)) and the reduced recharge model (figures 6(c) and 6(d)) are shown. For both models the estimated hydraulic conductivity is equal to the preferred value over large portions of the model domain (corresponding to a value of -0.712 on a log-scale), while higher values are obtained in the pasture area, where rainwater infiltrates. As can be seen, lower conductivities were estimated in the reduced recharge model compared to the full recharge model, due to the lower net average influx rate (272 mm $year^{-1}$ for the full model compared to 42 mm $year^{-1}$ for the reduced one). Indeed, at lower infiltration rates lower hydraulic conductivities are required in the pasture area to drain the incoming recharge flux.

In Figure 8, slug test estimates are compared with those obtained from the flow inversions. The hydraulic conductivities estimated using the full recharge model are higher than those obtained from the slug-in tests, in particular in the pasture area (with a peak value of 15.31 m d^{-1} close to piezometer 16). For the reduced recharge model the estimated hydraulic conductivities in the factory area lies more realistically between the slug in and slug out estimates and the overestimation in the pasture area (piezometers 10 to 17) is reduced, in particular at piezometer 16. In the reduced recharge model elevated hydraulic conductivity values were estimated at the north boundary (with a peak of 3.41 m d^{-1}), where the groundwater flow is poorly characterized (few head measurements available).

Despite the reduction of the infiltration rate at the water table in the reduced recharge model, discrepancies between the hydraulic conductivities estimated with pilot points and slug data still persist. A similar result was found by Kowalsky et al. (2012) and was attributed to a possibly incorrect analysis of the slug data, such as the specification of the influence radii, or the different averaging of the hydraulic conductivities in the slug tests and pilot point estimations. Moreover, the hydraulic conductivities estimated with the slug out data are four times lower than those obtained

from the slug in data, confirming that these tests can only provide approximate hydraulic conductivity estimates (Campbell et al., 1990).

In Figure 6(b) and 6(d) the inferred specific yield values are shown. For the full recharge model, specific yield ranges from 0.009 to 0.966, with extreme values close to piezometer 5. These high values are outside the upper bound suggested for sandy clay soils and might indicate the presence of model errors (Hill and Tiedeman, 2007). The large variations of the influent fluxes in the full recharge model cause large fluctuations of water levels in the pasture area and in the nearby factory area, which are compensated for by using high specific yield values (Figure 6(b)). In the reduced recharge model these extreme values are eliminated, yielding a minimum specific yield value of 0.011 in the pasture area and a maximum value of 0.164 in the factory area, which are more plausible for a sandy clay soil. In the areas where no groundwater levels measurements were taken, the specific yield values are close to the preferred value (0.1), imposed by the regularization constraints.

Overall, the reduced recharge model appears more appropriate from the results obtained for the hydraulic conductivity and specific yield. This interpretation could not have been made only based on the fit of the groundwater levels obtained in Figure 7, where both recharge models fit the calibration data similarly, with an RMSE value close to the 0.15 m target ($\Phi^{l}_{m,1}$ equal to 9.45). The validation cross plots include some outliers, which considerably increase the RMSE (Figure 7(b) and 7(d)). These measurements were taken close to the barrier before its installation, and they are up to 2 meters lower than post-barrier installation measurements and therefore could have been wrongly measured (for example, due to the misspecification of the piezometer elevation).

While the parameter values seem to suggest the reduced recharge model as the most appropriate, information from the concentration data are also required to support this hypothesis.

Figure 9 compares simulated total contaminant concentrations assuming no biodegradation and using the two recharge models. In these tests the effective porosity, the longitudinal dispersivity and the release rates at the sources were set to 0.1, 5 m and 1.5e-4 mol L^{-1} d^{-1} respectively

(corresponding to a total released mass at each source of 1000 kg). The model simulations were extracted at the 2009-2012 sampling events and averaged. The average measured and simulated values were interpolated using inverse-distance-squared method. In this manner the maps of the average simulated concentrations can directly be compared with the maps of the average measured values.

From Figure 9 it is evident that the contaminant plumes in the pasture area as well as the concentrations at source 3 are underestimated when using the full recharge model, even assuming no biodegradation. Even when a higher contaminant mass was released at the sources (10000 kg at each source) and a higher mass transfer was used (1e-3 d^{-1}), the contaminant concentrations in the pasture area were underestimated and in the factory area largely overestimated. This result indicates that the underestimation of contamination in the pasture with the full recharge model is not due to underestimation of the released mass but to excessive dilution by infiltrating rainwater. Using the reduced recharge model (Figure 9(c)), the dilution effect in the pasture area and at source 3 is reduced. The contaminant plume originating from source 3 is clearly divided after the barrier installation, as confirmed by measured concentrations at piezometer 10, where an abrupt decline of pollutant concentrations was measured after barrier installation (results not shown). The plume separation can also be seen in Figure 9(a), where two highly polluted areas are present before and after the barrier, corresponding to source 3 and the detached plume.

The results obtained with the reduced recharge model are more consistent with the concentration measurements compared to the full recharge model, as already indicated by the more realistic flow parameters in the first step. With regard to contaminant dilution in the pasture area, an alternative to reducing recharge would be to introduce different hydraulic conductivity values for the top and bottom layer. We tested this hypothesis by repeating the flow optimization (step 1), using a preferred hydraulic conductivity value for the bottom layer equal to the average value of the slug tests (since most of the slug tests were performed in piezometers screened in the deep layer) and a ten times higher hydraulic conductivity value for the top layer. Enforcing hydraulic conductivity

differences between the two layers resulted in a slightly worse fit to measured heads (0.156 m in calibration and 0.347 m in validation), but partially avoided contaminant dilution. However, concentrations in the source areas were overestimated due to the lower hydraulic conductivity (and effective velocities) in the deep layer. Moreover, the hydraulic conductivities in the top layer appeared too high, as indicated by the difference between the slug in estimate in the shallow piezometer 10 (0.15 m d^{-1}) and the corresponding estimation obtain through inverse modelling (1.763 m d^{-1}).

From the results obtained with the conservative transport experiments it is evident that the reduced recharge model is more appropriate as it avoids the strong dilution effect simulated with the full recharge model, resulting in severe underestimation of contaminant spreading, even without accounting for sorption or biodegradation. The results highlight the importance of considering different data types when estimating model parameters, eventually disregarding model formulations that lead to poor simulated concentrations.

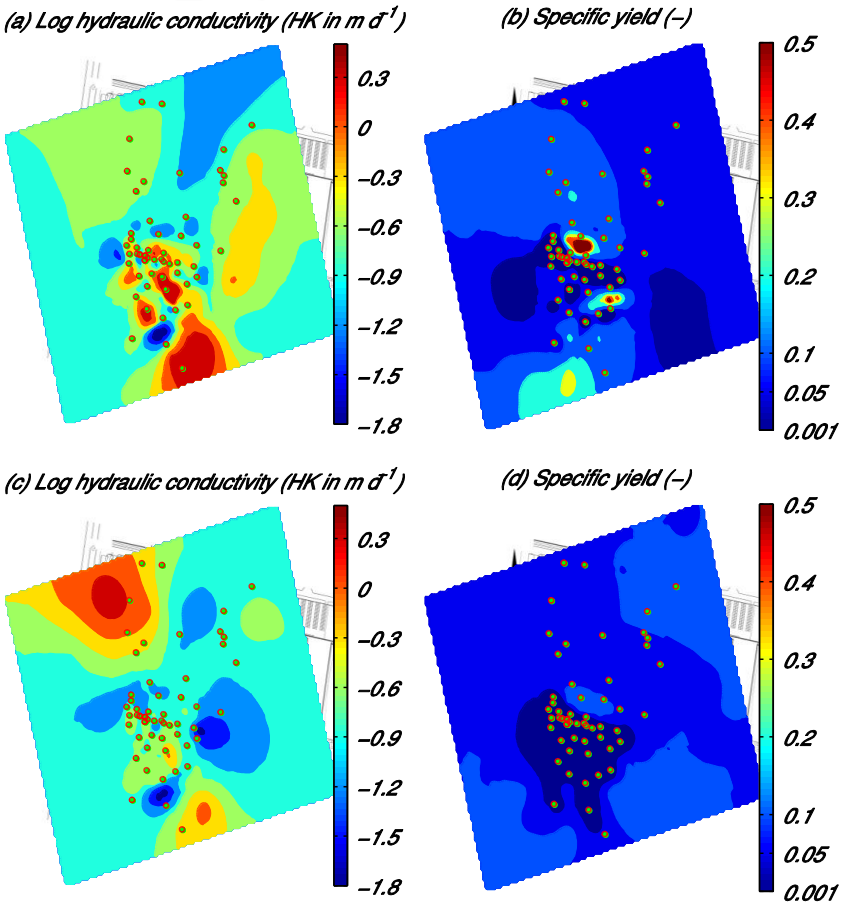

Figure 6: (a) Horizontal hydraulic conductivity and (b) specific yield estimated with the full recharge model, (c) horizontal hydraulic conductivity and (d) specific yield estimated with the reduced recharge model.

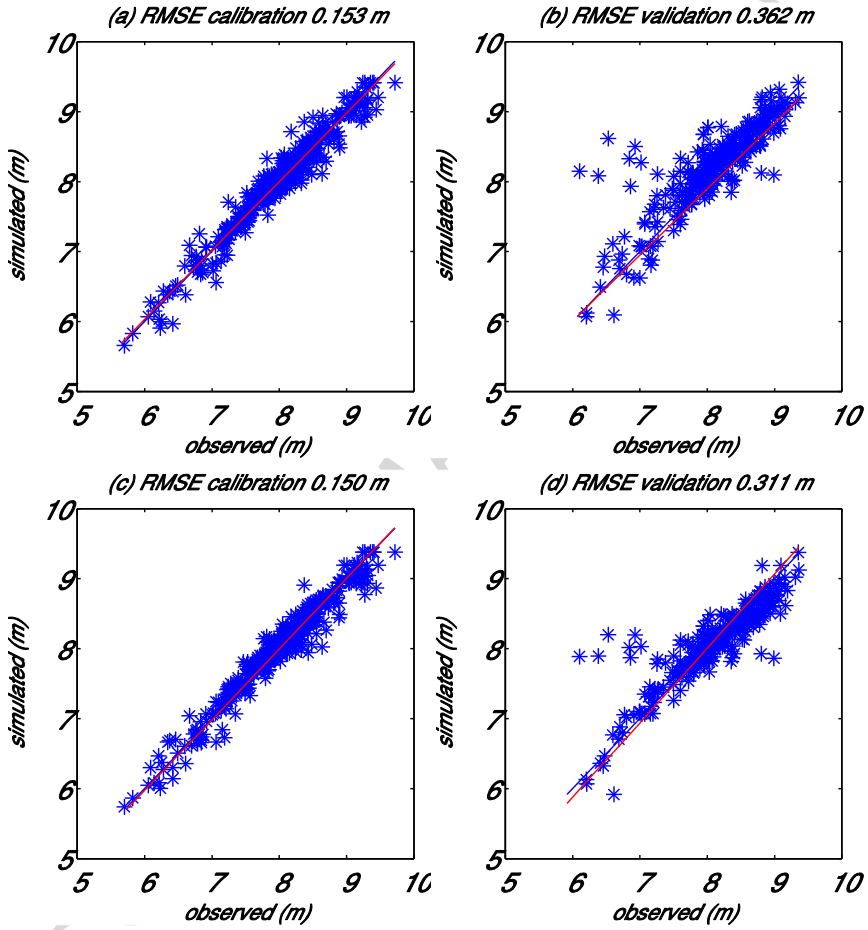

Figure 7. (a) Cross plot in calibration and (b) validation with the full recharge model, (c) cross plot in calibration and (d) validation with the reduced recharge model.

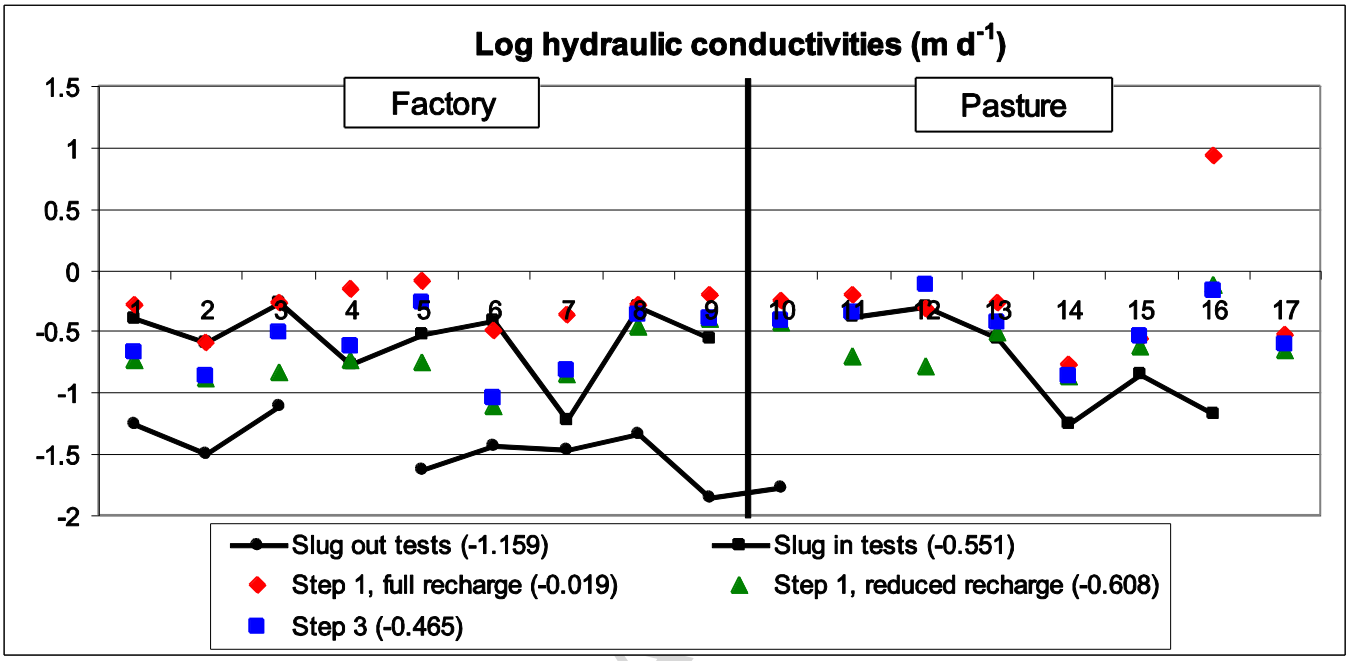

Figure 8. Estimated log-transformed hydraulic conductivities from slug tests and from parameter optimizations (piezometers locations are indicated in Figure 1). Values in brackets within the legend indicate the arithmetic averages.

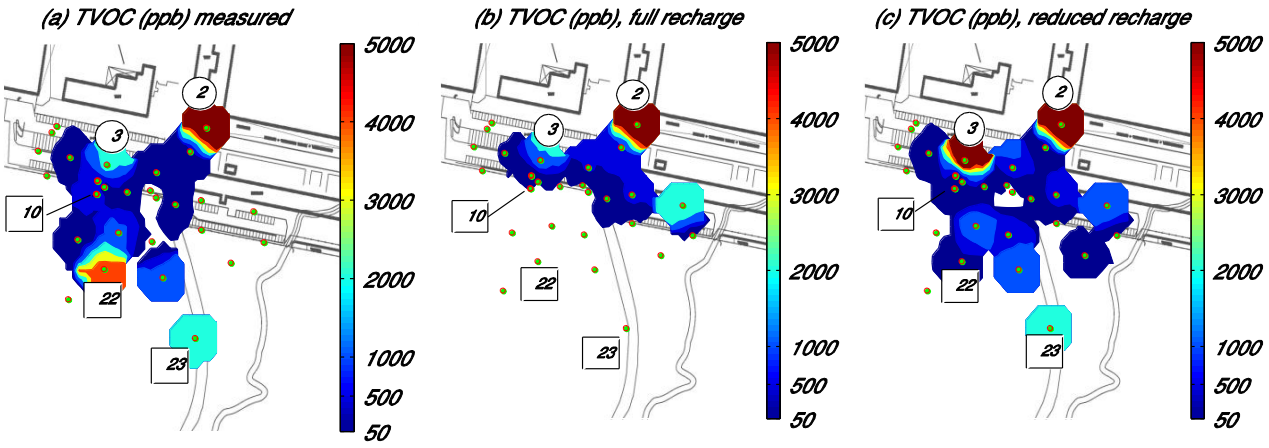

Figure 9. (a) Total average contaminant concentration measured in the 2009-2012 period, (b) total average contaminant concentration simulated using the full recharge model and (c) total average contaminant concentration simulated using the reduced recharge model. Source locations are indicated by numbered circles and piezometer numbers by numbered rectangles.

4.3 Step 2: refinement of reactive transport parameters

In this step, reactive transport parameters were estimated from concentration data, fixing the flow field as determined in step 1 and using the reduced recharge model. Figure 10 shows that most of the estimated model parameters (white bars) are lower than the initial parameter guesses (black bars). As can be seen a large value of the longitudinal dispersivity (56.11 m) was estimated, yielding a wide spread of the VC plume (Figure 12(c)). From the Figure it is evident that the longitudinal and transversal dispersivities must be reduced. Moreover, the estimated effective porosity (0.57) is above the total porosity estimated from core samples (0.4).

The estimated biodegradation coefficients estimated in this optimization step are very low (Figure 10), up to 2 orders of magnitude lower than those estimated from the lab experiments. Such discrepancy between the rates estimated in lab and site conditions is consistent with previous studies (Suarez and Rifai, 1999). A low value was also estimated for the $f_{s/VOC}$ parameter (5.06), indicating a small consumption of the organic substrate by dechlorinators and an almost constant $\mu_k S$ product in Equation 9, as used in most field scale models (Clement et al., 2000; D'Affonseca et al., 2011). On the other hand, this results contradicts the correlation found in the batch experiments between the low organic carbon content at piezometer 9, 10, 21 and 16 (< 0.3%) and the observed low biodegradation rates, suggesting the need for more investigations of the organic carbon consumption mechanism at the site.

In the optimization of reactive transport parameters compromises in fitting different species were observed. For example the simulated PCE concentrations at source 1 were overestimated and TCE concentrations underestimated (figure 10). Only few PCE and TCE measurements were taken close to source 1 (3 for PCE and 3 for TCE before the barrier installation) and their influence on the estimation was small, amounting to 8.6% of the total PCE and TCE composite sensitivity. Close to source 3, more measurements were taken, with a larger contribution to PCE and TCE composite sensitivity (about 64.1%). Since the measurements at source 3 are more sensitive and matching the

TCE concentrations at source 1 would cause an overestimation of TCE concentrations at source 3, the inversion algorithm fitted the TCE and PCE measurements at source 3 more closely. Compromises in fitting the same specie at different locations were also observed. An example is the cis-DCE plume originating from the sources 1 and 3, which is correctly oriented but strongly underestimated in the pasture area (piezometer 22). In this case most of the cis-DCE composite sensitivity belongs to the high concentration measurements close to source 2 (30.6%) and source 3 (14.2%) and it was difficult to match these measurements simultaneously to those collected in the pasture (amounting to 9.0% of the total cis-DCE composite sensitivity).

Estimating additional parameters (e.g. flow parameters) using concentration data could reduce these tradeoffs and improve the fitting of each contaminant plume in different areas. Of particular interest is reproducing the VC pollution at source 2 and piezometer 23, which is largely underestimated after step 2 (Figure 11(h)). A correct simulation of the VC pollution at piezometer 23 is important because VC is the most mobile and toxic chlorinated compound.

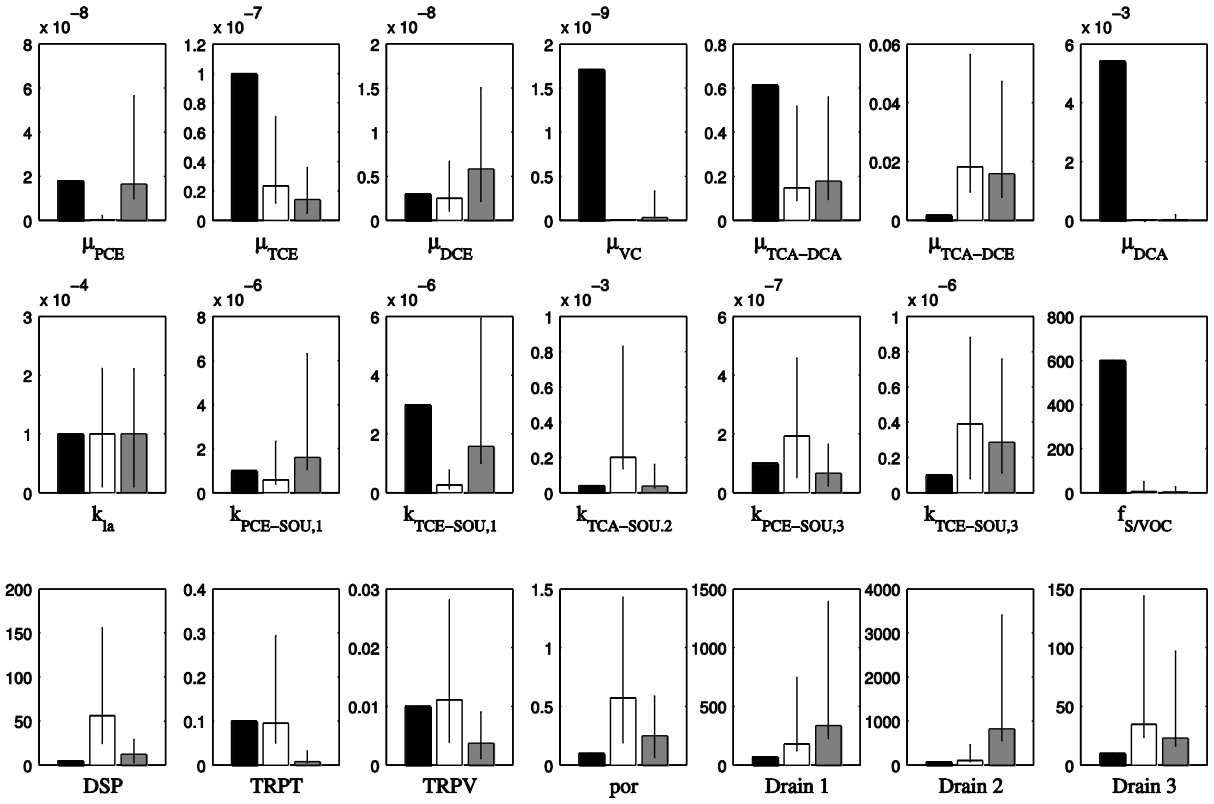

Figure 10. Initial parameter values (black bars), optimal values after step 2 (white bars) and after step 3 (gray bars). Vertical lines indicate the 95% confidence intervals, estimated from the posterior covariance matrix. Parameter units are reported in Table 1.

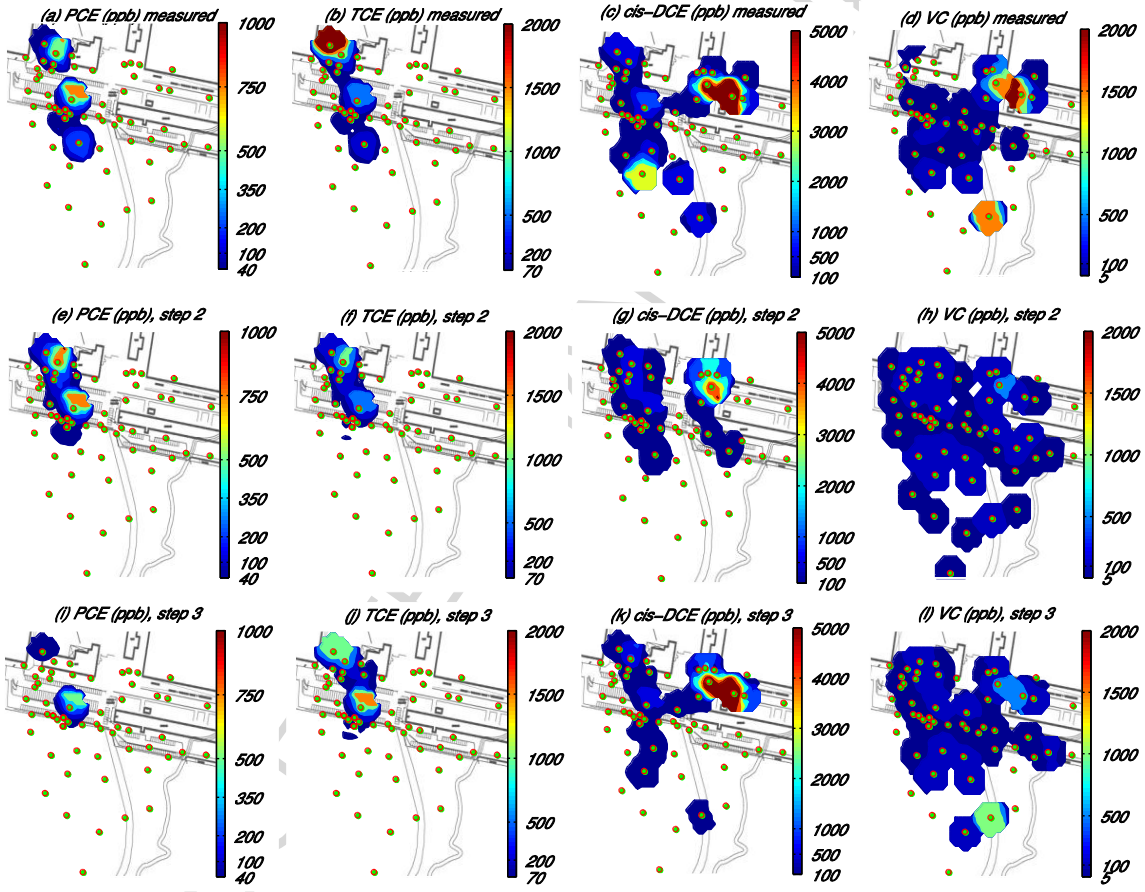

Figure 11. Average measured concentration maps (figures a-d), average simulated concentrations after step 2 (figures e-h), and average simulated concentrations after step 3 (figures i-l).

Table 2. Root mean squared errors achieved at each inversion step (RMSEs for contaminants are expressed in part per billion (ppb) and for groundwater heads in meters).

	PCE	TCE	cis-DCE	VC	TCA	DCA	Heads
Initial guess	182	351	1415	418	432	3068	0.150
Step 2	155	310	1366	454	114	2672	0.150
Step 3	186	323	989	354	115	2008	0.168
Target RMSEs step 3	200	300	1000	300	200	2000	0.150

4.4 Step 3: refinement of all parameters from all field data

In this step reactive transport and flow parameters were estimated simultaneously, using the 2011 head data and all concentration measurements. The initial flow parameters values were obtained from step 1, whereas the initial values of the reactive transport parameters were equal to those estimated in the initial guess (black bars in Figure 10). The flow field estimated in step 1 ensures a correct orientation of the plume and non-zero sensitivity of the measurements with respect to the parameters (Schwede and Cirpka, 2009). Specific yield parameters were kept fixed to the values obtained in step 1 because their sensitivity at the initial parameter estimate was small (more than 172 times smaller than the maximum composite sensitivity). The reactive transport parameters estimated after step 2 could also be used as initial values for step 3 (dashed arrow in Figure 5). However, it was found that step 3 optimization was not able to converge to realistic porosity and dispersivity values within the maximum number of iterations, mainly because the initial values were far from being realistic. Therefore, the initial values of the reactive transport parameters at step 3 were set equal to the initial guess.

Estimating more parameters should result in an improved fit to the measurements compared to step 2. This was observed for the most mobile species such as cis-DCE, VC and TCA, which are affected the most by local variations of the flow field (Table 2 and Figure 11). In step 3 the average

VC concentrations at piezometer 23 are also better reproduced (compare Figure 11(d) with Figure 11(l)). High VC concentrations in this area were also caused by a negative recharge flux, as larger evaporative fluxes were simulated in areas with shallow groundwater table. This was verified using the ZONEBUDGET program (Harbaugh, 1990). The amount of rainwater infiltrating in the area close to piezometer 23 during the period 1957-2000 (first steady state stress period) amounts to 160.22 mm y^{-1} whereas simulated evaporation is 278.32 mm y^{-1}, yielding a negative imbalance of -118.11 mm y^{-1} and indicating that the downslope portion of the pasture functions as a groundwater discharge area, a finding that should be confirmed with in-situ infiltration measurements.

The target RMSEs values listed in Table 2 were determined from preliminary runs, testing the maximum achievable fit and assessing the plausibility of the obtained hydraulic conductivity fields. Low targets make the inverse problem unstable (hydraulic conductivity fields with high variances) because the $\beta^2\Phi r$ term in Equation (18) becomes underweighted. Moreover, it was found that low targets not always resulted in lower RMSEs, with an increase of the measurement objective function ($\sum_{j=1}^{7}\Phi_{m,j}$ in Equation (18)) after the first optimization iterations. Specifying low targets for a specific set might also impede the achievement of the specified targets for other sets. This was observed for PCE and TCE, where low TCE target worsen the PCE fit.

The degradation parameters obtained after step 3 are similar to those obtained after step 2 (compare white and gray bars in the top row of Figure 10), except for an increased μ_{PCE} coefficient, which caused an underestimation of PCE concentrations at source 1 and 3 (Figure 11(i)) and an increased RMSE for PCE (Table 2). The estimated released DNAPL mass at source 3 decreased compared to the estimation provided at step 2 (from 34 kg to 8 kg). This lower estimation might indicate an accidental spillage not related to a particular production activity, as suggested by historical information on the production areas. A compressor test area is reported at source 1 and confirmed by higher release coefficients, with a total released DNAPL mass of 79 kg. The release rate at

source 2 was reduced compared to the estimation provided by step 2 (from 10140 kg to 860 kg) with a narrower confidence interval. In the previous optimization, $k_{TCA\text{-}SOU,2}$ was strongly increased from the initial guess to match the high concentrations measured at piezometer 19, despite the incorrect orientation of the cis-DCE plume (Figure 11(a)).

The most striking feature of optimizing flow and transport parameter simultaneously is the reduction of the longitudinal dispersion coefficient compared to the separate flow and transport optimizations (Figure 12), due to a better representation of the hydraulic conductivity heterogeneity. Similar results were also found by Tonkin and Doherty (2005) and it agrees with a lowering of mechanical dispersion as more heterogeneity is explicitly accounted for in the model (Carrera, 1993; Konikow, 2011). A more realistic value of the effective porosity (0.25) was also estimated in step 3.

The question remains whether the estimated hydraulic conductivity fields are realistic. The hydraulic conductivity fields in the polluted area before and after step 3 are shown in Figure 13(a) and 13(b). As can be seen from the figures, the low hydraulic conductivities formations identified from head data at piezometer 25 and on the right part of the barrier are retained after step 3, with point-scale hydraulic conductivity estimates similar to those obtained from slug-in tests (Figure 8). Most of the differences between the two fields are located in the source areas, with maximum hydraulic conductivity values close to source 2, to correct the plume direction towards piezometer 19 and the central part of the barrier (Figure 12(a,b)). These estimates should be supported by additional field measurements because they might also compensate for an incorrect localization of the second source.

Similarly to the hydraulic conductivity fields, also the infiltration patterns show large variation over short distances to attempt a better fit to the measurements. Figure 13(c) shows the estimated infiltration rate after step 1 and Figure 13(d) after step 3. As can be seen, in step 1 (using only head data) the homogeneous regularization constraint is respected, whereas after step 3 (head and concentration data) a heterogeneous field was estimated, with the lowest value between piezometer

16 and 24 (0.062), the latter at the fringe of the VC plume (Figure 12(d)). This low value indicates that almost no water infiltrates and seems to represent an inversion artefact rather than a realistic infiltration rate at the site, because larger recharge rates are expected for deep water tables, as opposed to the obtained results, where a lower infiltration fraction was estimated in zones of deeper groundwater table (about 1 m). As mentioned above, infiltration measurements are required to corroborate the estimations of the recharge parameters.

The additional information content of the concentration data on the flow parameters was quantified by estimating the reduction of the posterior parameter uncertainty. The posterior standard deviation fields for hydraulic conductivity and infiltration fractions are shown in Figure 14. The standard deviation fields were obtained extracting the diagonal elements of the posterior covariance matrix and by kriging the square root values as done for hydraulic conductivity pilot points. Figure 14 shows that prior standard deviations for hydraulic conductivity (0.5) and infiltration fraction (0.251) were reduced over larger areas when concentration measurements were also used in the estimation, as opposed to using only head measurements. This is due to the assimilation of the extensive concentration dataset but also to the proprieties of contaminant concentrations, which contain non punctual information on hydraulic properties. However, the maximum reduction of the prior standard deviation at step 1 and 3 was similar: for hydraulic conductivity the maximum reduction is 72.8 % for step 1 and 73% for step 3 and for infiltration the fraction is 71.6% and 74.7% respectively.

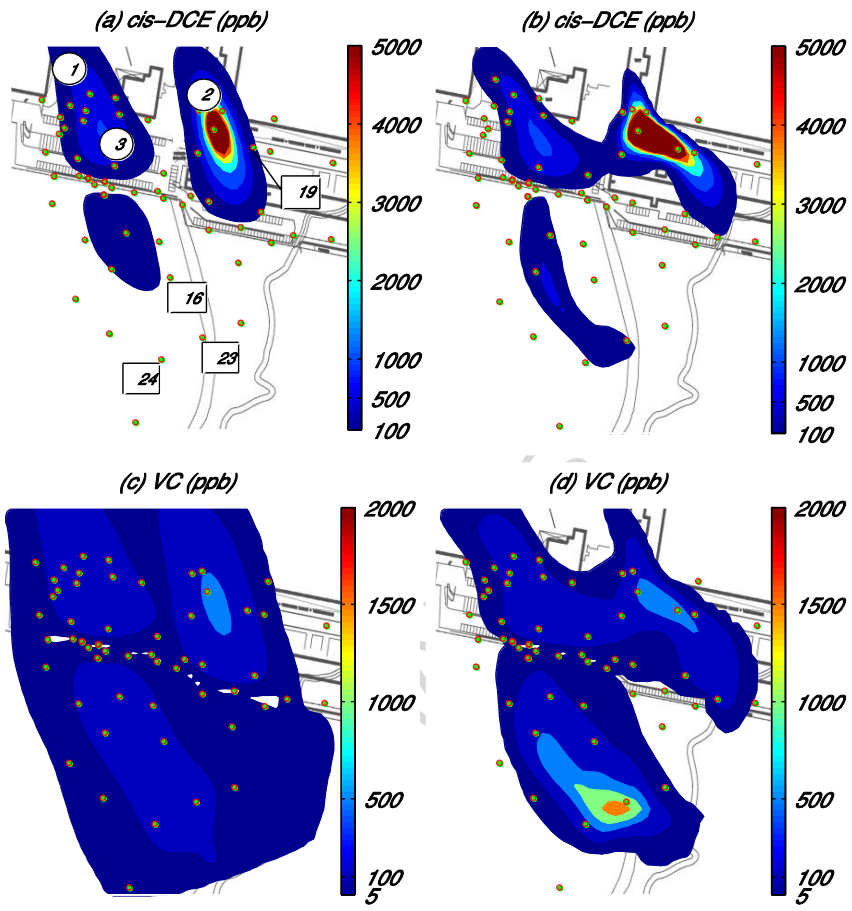

Figure 12. cis-DCE and VC plumes at 01-01-2012 after separate estimation of flow and transport parameters (step 2, figures (a) and (c)) and after simultaneous estimation of flow and transport parameters (step 3, figures (b) and (d)). In Figure (a) the source locations are indicated by numbered circles and piezometer by numbered rectangles.

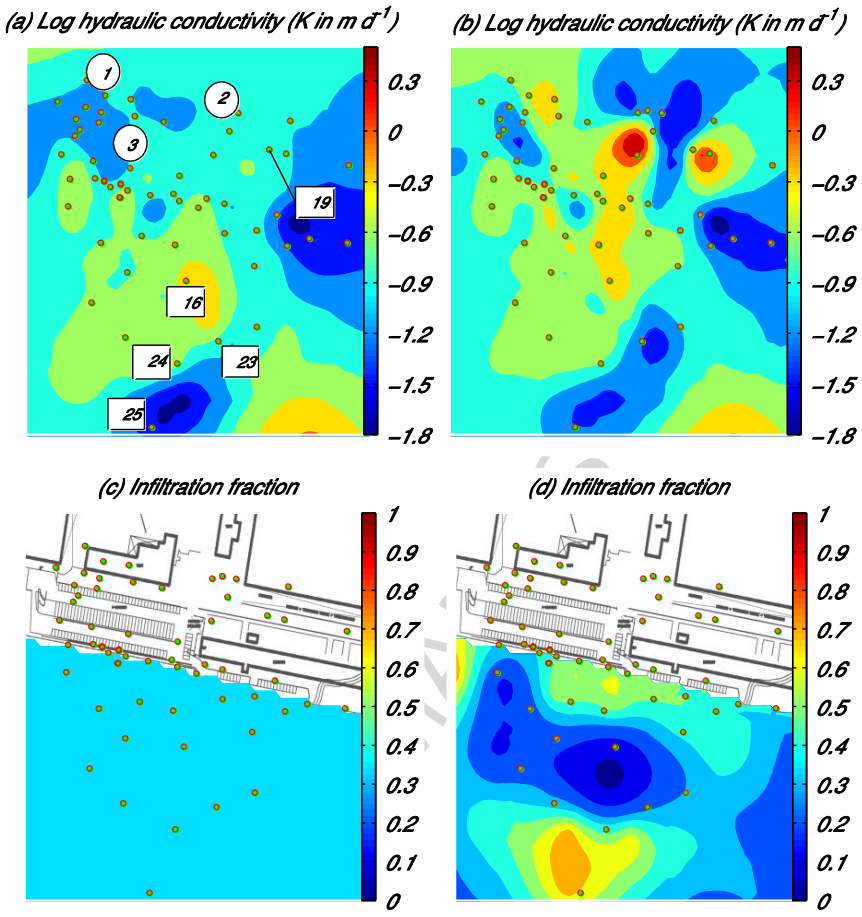

Figure 13. Hydraulic conductivity and infiltration fraction after separate estimation of flow and transport parameters (step 2, figures (a) and (c)) and after simultaneous estimation of flow and transport parameters (step 3, figures (b) and (d)). In Figure (a) the source locations are indicated by numbered circles and piezometers by numbered rectangles.

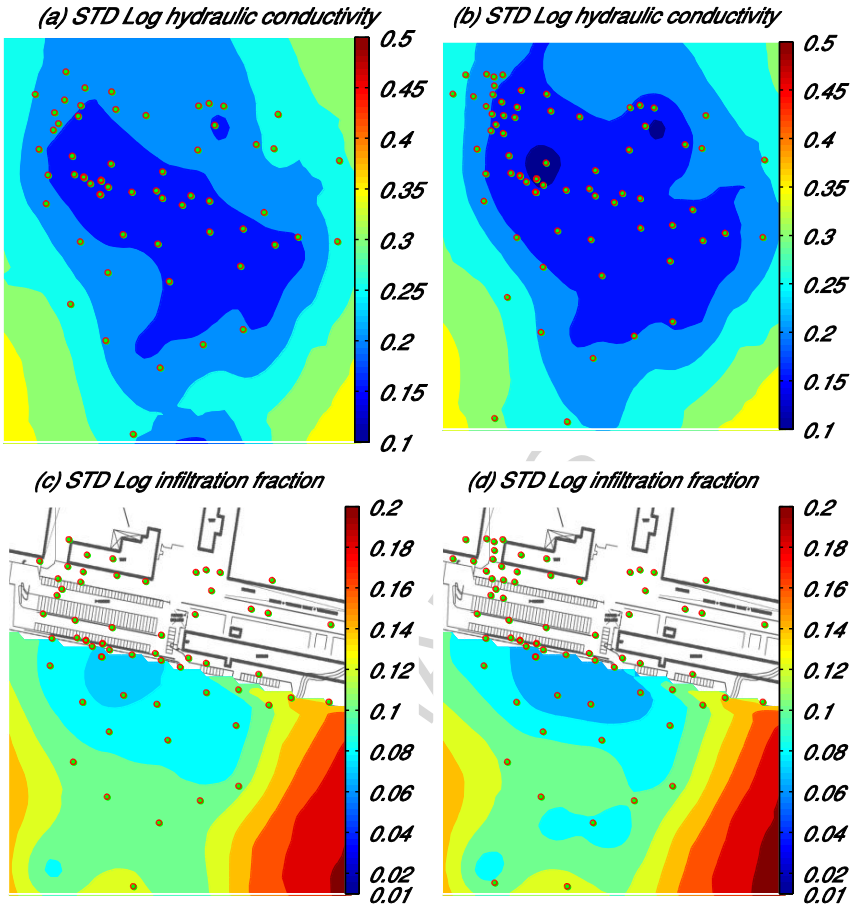

Figure 14. Standard deviation of log hydraulic and log infiltration fraction after separate estimation of flow and transport parameters (step 2, figures (a) and (c)) and after simultaneous estimation of flow and transport parameters (step 3, figures (b) and (d)). For all fields the same prior covariance and observation weights were used.

The analysis of concentration time series at selected piezometer locations reveals that the observed temporal variations could not be reproduced and the best simulations that could be obtained are concentration time series passing through the measurements. This could be due to the use of temporally averaged (weekly) values for precipitation and evaporation. Part of the observed variations might also be attributed to unaccounted processes during the data collection (for example the volatilization of contaminants during the sampling). Finally, model errors (e.g. unmodeled unsaturated zone dynamics and the description of the contaminant release from the sources) are likely to be important as well. Good average simulated results were obtained for VC concentrations

at piezometer 23 (Figure 11(l)). Simulated VC concentrations indicate that in the year 2035 VC concentrations might be as high as the ones measured during 2002-2011, due to the small effect of contaminant dilution and degradation.

5. Discussion and Conclusions

In this work a multicomponent reactive transport model of a permeable reactive barrier site was developed and calibrated to reproduce the present and future contamination. The model includes the processes considered important for the reproduction of the observed pollution, including different recharge patterns in the factory and in the pasture area, contaminant biodegradation and abiotic degradation in the reactive barrier. Two alternative groundwater recharge models were tested (full and reduced recharge) and hydraulic conductivity, specific yield and infiltrating precipitation fractions were parameterized with pilot points, allowing the mapping of the expected parameter variability in the model domain. Flow parameters were estimated from head measurements (step 1), followed by optimization of reactive transport parameters from concentration measurements (step 2). In an additional test (step 3), flow and reactive transport parameters were inferred from head and concentration measurements. Parameter and prediction uncertainties were also estimated, assuming known prior parameter covariance and linearizing the model at the optimum parameters.

Recharge in this shallow groundwater system plays a crucial role in contaminant migration. Our results indicate that the two recharge models fit the head data similarly well, with different estimates for spatially variable hydraulic conductivity and specific yield. However, when using the full recharge model, contamination in the pasture area was strongly diluted, even when neglecting sorption and biodegradation, and assuming elevated source release rates. The reduced recharge model avoids this problem by generating less contaminant dilution and yielding estimates for hydraulic conductivity and specific yield that more closely correspond to measured values. Inferred infiltration rates are fairly low however, and in-situ infiltration measurements are required to verify the validity of this approach. Introducing layered heterogeneity in the model, as an alternative to the

reduced recharge model for reducing contaminant dilution in the bottom model layer, did not result in satisfying results, and thus the reduced recharge model was retained.

The use of pilot point parameterization introduced a large number of model parameters. To stabilize the inversion, mathematical (singular value decomposition, (Aster et al., 2005)) and explicit regularization (Ory and Pratt, 1995; Tikhonov et al., 1977) were imposed to the parameter fields. Singular value decomposition had a negligible regularization effect, due lo the small cutting threshold used in the experiments (1e-6). More relevant was the effect of the explicit regularization constrains on the parameter inference. The weight of the regularization term in the objective function was adjusted iteratively to achieve specified fits to the individual chemical compounds. This fit was expressed by target objective functions which have a strong influence on the final parameter estimation, and thus need to be carefully chosen. Such problem was also recognized by Fienen et al. (2009 (b)), where it was stated that changes in regularization constraints (i.e. specific fitting targets) can result in very different parameter fields. In our application, the target objective function values were determined from preliminary model runs. As these values reflect expected misfits between model and data, they account for both measurement and model errors. In our case the model was able to reproduce spatial patterns of time-averaged concentrations, but did not adequately mimic temporal variation of measured concentration at individual piezometers.

The advantage of introducing a flexible parameterization of flow parameters (in particular hydraulic conductivity) is that measured concentrations can be better reproduced. The best matches between measured and simulated cis-DCE and VC plumes were obtained when head and concentration data were used to estimate model parameters. Concentration data contained information about hydraulic conductivity and infiltrating rainwater fractions also in the impervious model area, as demonstrated by the larger reduction of the prior parameters standard deviations compared to the separate estimation of flow and transport parameters. Moreover, a more realistic estimation of the effective porosity and a reduction of the dispersion coefficients were obtained in the joint inversion, in agreement with previous modelling studies (Tonkin and Doherty, 2005). However, some features

of the infiltrating fraction and hydraulic conductivity fields might represent an inversion artefact. For example, large variations of hydraulic conductivity were estimated close to the second source and might compensate for an incorrect localization of the source.

To provide more reliable predictions, the current description of flow and transport processes at the site should be improved using additional information, as indicated from the results of this first modelling effort. These include: (1) direct infiltration measurements in the pasture area, (2) additional concentration measurements between source 2 and the second barrier segment, (3) a precise quantification of the measurement error beyond the analytical uncertainty, and (4) biodegradation tests in additional piezometers to confirm the current description of the biodegradation process.

Ongoing research aims to integrate a geochemical passivation model developed on lab experiments into the field scale model, in order to quantify the impact of declining barrier reactivity on future contaminant migration. From the results obtained in this study a correct description of the water balance is also crucial to predict long-term contamination at the site. In our specific case, reactive transport modelling improved the conceptual understanding of flow and contaminant migration at the site.

Acknowledgments

Funding for this research was provided by the European Community in the context of the AQUAREHAB Project (FP7-ENV-2008.3.1.1.1). We would like to thank NWO for providing high performance computing resources (project number MP-253-12).

References

Arnold, W.A. and Roberts, A.L., 2000. Pathways and Kinetics of Chlorinated Ethylene and Chlorinated Acetylene Reaction with Fe(0) Particles. Environmental Science & Technology, 34(9): 1794-1805.

Assefa, K.A. and Woodbury, A.D., 2013. Transient, spatially varied groundwater recharge modeling. Water Resources Research, 49(8): 4593-4606.

Aster, R., Borchers, B. and Thurber, C., 2005. Parameter estimation and inverse problems: Elsevier Academic Press. Burlington, Massachusetts.

Bauer, M., Heitmann, T., Macalady, D.L. and Blodau, C., 2006. Electron Transfer Capacities and Reaction Kinetics of Peat Dissolved Organic Matter. Environmental Science & Technology, 41(1): 139-145.

Burnett, R.D. and Frind, E.O., 1987. Simulation of contaminant transport in three dimensions: 2. Dimensionality effects. Water Resources Research, 23(4): 695-705.

Campbell, M.D., Starrett, M.S., Fowler, J.D. and Klein, J.J., 1990. Slug test and hydraulic conductivity. Ground Water Manage, 4: 85-99.

Carniato, L. et al., 2012. Predicting longevity of iron permeable reactive barriers using multiple iron deactivation models. Journal of Contaminant Hydrology, 142–143(0): 93-108.

Carrera, J., 1993. An overview of uncertainties in modelling groundwater solute transport. Journal of Contaminant Hydrology, 13(1–4): 23-48.

Carrera, J., Alcolea, A., Medina, A., Hidalgo, J. and Slooten, L.J., 2005. Inverse problem in hydrogeology. Hydrogeology Journal, 13(1): 206-222.

Certes, C. and de Marsily, G., 1991. Application of the pilot point method to the identification of aquifer transmissivities. Advances in Water Resources, 14(5): 284-300.

Clapp, L., Semmens, M., Novak, P. and Hozalski, R., 2004. Model for In Situ Perchloroethene Dechlorination via Membrane-Delivered Hydrogen. Journal of Environmental Engineering, 130(11): 1367-1381.

Clement, T.P., 1997. RT3D: A Modular Computer Code for Simulating Reactive Multi-Species Transport in 3-Dimensional Groundwater Aquifers, Pacific Northwest National Laboratory, Richland, Washington.

Clement, T.P., Johnson, C.D., Sun, Y., Klecka, G.M. and Bartlett, C., 2000. Natural attenuation of chlorinated ethene compounds: model development and field-scale application at the Dover site. Journal of Contaminant Hydrology, 42(2–4): 113-140.

D'Affonseca, F.M., Prommer, H., Finkel, M., Blum, P. and Grathwohl, P., 2011. Modeling the long-term and transient evolution of biogeochemical and isotopic signatures in coal tar–contaminated aquifers. Water Resour. Res., 47(5): W05518.

Distefano, T.D., Gossett, J.M. and Zinder, S.H., 1992. Hydrogen as an Electron-Donor for Dechlorination of Tetrachloroethene by an Anaerobic Mixed Culture. Applied and Environmental Microbiology, 58(11): 3622-3629.

Doherty, J., 2003. Ground Water Model Calibration Using Pilot Points and Regularization. Ground Water, 41(2): 170-177.

Doherty, J., 2007. PEST: Model Independent Parameter Estimation, Watermark Numerical Computing, Brisbane, Australia.

Doherty, J. and Skahill, B.E., 2006. An advanced regularization methodology for use in watershed model calibration. Journal of Hydrology, 327(3–4).

Doherty, J.E., Fienen, M.N. and Hunt, R.J., 2010. Approaches to highly parameterized inversion: Pilot-point theory, guidelines, and research directions: U.S. Geological Survey Scientific Investigations Report 2010–5168, 36 p.

Fienen, M., Hunt, R., Krabbenhoft, D. and Clemo, T., 2009 (b). Obtaining parsimonious hydraulic conductivity fields using head and transport observations: A Bayesian geostatistical parameter estimation approach. Water Resour. Res., 45(8): W08405.

Fienen, M.N., Muffels, C.T. and Hunt, R.J., 2009 (a). On Constraining Pilot Point Calibration with Regularization in PEST. Ground Water, 47(6): 835-844.

Gallagher, M.R. and Doherty, J., 2007. Parameter interdependence and uncertainty induced by lumping in a hydrologic model. Water Resources Research, 43(5): W05421.

Gorelick, S.M., Evans, B. and Remson, I., 1983. Identifying sources of groundwater pollution: An optimization approach. Water Resour. Res., 19(3): 779-790.

Gupta, H.V., Clark, M.P., Vrugt, J.A., Abramowitz, G. and Ye, M., 2012. Towards a comprehensive assessment of model structural adequacy. Water Resources Research, 48(8).
Harbaugh, A.W., 1990. A computer program for calculating subregional water budgets using results from the US Geological Survey modular three-dimensional finite-difference ground-water flow model. US Geological Survey.
Harbaugh, A.W., Banta, E.R., Hill, M.C. and McDonald, M.G., 2000. MODFLOW-2000, the U.S. Geological Survey modular ground-water model—User guide to modularization concepts and the ground-water flow process, U.S. Geol. Surv. Open File Rep., 00-92, 121 pp.
Haston, Z.C. and McCarty, P.L., 1998. Chlorinated Ethene Half-Velocity Coefficients (KS) for Reductive Dehalogenation. Environmental Science & Technology, 33(2): 223-226.
Hayley, K., Schumacher, J., MacMillan, G.J. and Boutin, L.C., 2014. Highly parameterized model calibration with cloud computing: an example of regional flow model calibration in northeast Alberta, Canada. Hydrogeology Journal: 1-9.
He, J.Z. et al., 2002. Acetate versus hydrogen as direct electron donors to stimulate the microbial reductive dechlorination process at chloroethene-contaminated sites. Environmental Science & Technology, 36(18): 3945-3952.
Hill and Tiedeman, 2007. Effective groundwater model calibration: with analysis of data, sensitivities, predictions, and uncertainty. John Wiley & Sons.
Hill, M.C., 2006. The Practical Use of Simplicity in Developing Ground Water Models. Ground Water, 44(6): 775-781.
Hill, M.C. et al., 2013. Knowledge, transparency, and refutability in groundwater models, an example from the Death Valley regional groundwater flow system. Physics and Chemistry of the Earth, Parts A/B/C, 64(0): 105-116.
Hoeksema, R.J. and Kitanidis, P.K., 1984. An Application of the Geostatistical Approach to the Inverse Problem in Two-Dimensional Groundwater Modeling. Water Resources Research, 20(7): 1003-1020.
Hunt, R.J., Doherty, J. and Tonkin, M.J., 2007. Are Models Too Simple? Arguments for Increased Parameterization. Ground Water, 45(3): 254-262.
Hunt, R.J. et al., 2010. Using a Cloud to Replenish Parched Groundwater Modeling Efforts. Ground Water, 48(3): 360-365.
Johnson, A.I., 1963. Specific yield-Compilation of specific yield for various materials U.S. Geological Survey, Water-Supply Paper, 1662-D.
Johnson, C.D. and Truex, M.J., 2006. RT3D Reaction Modules for Natural and Enhanced Attenuation of Chloroethanes, Chloroethenes, Chloromethanes, and Daughter Products, Pacific Northwest National Laboratory, Richland, Washington.
Karlsen, R.H., Smits, F.J.C., Stuyfzand, P.J., Olsthoorn, T.N. and van Breukelen, B.M., 2012. A post audit and inverse modeling in reactive transport: 50 years of artificial recharge in the Amsterdam Water Supply Dunes. Journal of Hydrology, 454–455(0): 7-25.
Kitanidis, P.K. and Vomvoris, E.G., 1983. A geostatistical approach to the inverse problem in groundwater modeling (steady state) and one-dimensional simulations. Water Resources Research, 19(3): 677-690.
Konikow, L.F., 2011. The Secret to Successful Solute-Transport Modeling. Ground Water, 49(2): 144-159.
Kowalsky, M.B. et al., 2012. On parameterization of the inverse problem for estimating aquifer properties using tracer data. Water Resour. Res., 48(6): W06535.
Kowalsky, M.B. et al., 2011. Coupled modeling of hydrogeochemical and electrical resistivity data for exploring the impact of recharge on subsurface contamination. Water Resources Research, 47(2): W02509.
Laloy, E., Rogiers, B., Vrugt, J.A., Mallants, D. and Jacques, D., 2013. Efficient posterior exploration of a high-dimensional groundwater model from two-stage Markov chain Monte

Carlo simulation and polynomial chaos expansion. Water Resources Research, 49(5): 2664-2682.

Manoli, G. et al., 2012. A remediation performance model for enhanced metabolic reductive dechlorination of chloroethenes in fractured clay till. Journal of Contaminant Hydrology, 131(1–4): 64-78.

Marsily, G., 1984. Spatial Variability of Properties in Porous Media: A Stochastic Approach. In: J. Bear and M.Y. Corapcioglu (Editors), Fundamentals of Transport Phenomena in Porous Media. NATO ASI Series. Springer Netherlands, pp. 719-769.

Matott, L.S. and Rabideau, A.J., 2008. Calibration of complex subsurface reaction models using a surrogate-model approach. Advances in Water Resources, 31(12): 1697-1707.

McWhorter, D.B. and Sunada, D.K., 1977. Ground water hydrology and hydraulics. Water Resources Publication.

Ory, J. and Pratt, R., 1995. Are our parameter estimators biased? The significance of finite-difference regularization operators. Inverse Problems, 11(2): 397.

Pankow, J.F. and Cherry, J.A., 1996. Dense chlorinated solvents and other DNAPLs in groundwater, 522. Waterloo Press Portland Oregon.

Pollock, D. and Cirpka, O.A., 2012. Fully coupled hydrogeophysical inversion of a laboratory salt tracer experiment monitored by electrical resistivity tomography. Water Resour. Res., 48(1): W01505.

Prommer, H., Anneser, B., Rolle, M., Einsiedl, F. and Griebler, C., 2009. Biogeochemical and Isotopic Gradients in a BTEX/PAH Contaminant Plume: Model-Based Interpretation of a High-Resolution Field Data Set. Environmental Science & Technology, 43(21): 8206-8212.

RamaRao, B.S., LaVenue, A.M., De Marsily, G. and Marietta, M.G., 1995. Pilot Point Methodology for Automated Calibration of an Ensemble of conditionally Simulated Transmissivity Fields: 1. Theory and Computational Experiments. Water Resour. Res., 31(3): 475-493.

Rittmann, B.E. and McCarty, P.L., 2001. Environmental biotechnology. McGraw-Hill New York.

Rotter, B.E., Barry, D.A., Gerhard, J.I. and Small, J.S., 2011. Modeling the effectiveness of U(VI) biomineralization in dual-porosity porous media. Journal of Hydrology, 402(1–2): 14-24.

Schwarzenbach, R.P., Gschwend, P.M. and Imboden, D.M., 2005. Environmental organic chemistry. John Wiley & Sons.

Schwede, R.L. and Cirpka, O.A., 2009. Use of steady-state concentration measurements in geostatistical inversion. Advances in Water Resources, 32(4): 607-619.

Şengör, S.S. and Ünlü, K., 2013. Modeling contaminant transport and remediation at an acrylonitrile spill site in Turkey. Journal of Contaminant Hydrology, 150(0): 77-92.

Shah, N., Nachabe, M. and Ross, M., 2007. Extinction Depth and Evapotranspiration from Ground Water under Selected Land Covers. Ground Water, 45(3): 329-338.

Simunek, J., Van Genuchten, M.T. and Sejna, M., 2005. The HYDRUS-1D software package for simulating the one-dimensional movement of water, heat, and multiple solutes in variably-saturated media. University of California-Riverside Research Reports, 3: 1-240.

Suarez, M.P. and Rifai, H.S., 1999. Biodegradation Rates for Fuel Hydrocarbons and Chlorinated Solvents in Groundwater. Bioremediation Journal, 3(4): 337-362.

Sun, N.-Z., 1994. Inverse Problems in groundwater modeling, 6. Kluwer Academic.

Tikhonov, A.N., Arsenin, V.I. and John, F., 1977. Solutions of ill-posed problems. Winston Washington, DC.

Todd, D.K., 1959. Groundwater hydrology. J. Willey and Sons.

Tonkin, M. and Doherty, J., 2009. Calibration-constrained Monte Carlo analysis of highly parameterized models using subspace techniques. Water Resour. Res., 45(12): W00B10.

Tonkin, M.J. and Doherty, J., 2005. A hybrid regularized inversion methodology for highly parameterized environmental models. Water Resour. Res., 41(10): W10412.

Vandenbohede, A., Wallis, I., Houtte, E. and Ranst, E., 2013. Hydrogeochemical transport modeling of the infiltration of tertiary treated wastewater in a dune area, Belgium. Hydrogeology Journal, 21(6): 1307-1321.

Wagner, B.J., 1992. Simultaneous parameter estimation and contaminant source characterization for coupled groundwater flow and contaminant transport modelling. Journal of Hydrology, 135(1-4): 275-303.

Wiedemeier, T.H., Rifai, H.S., Newell, C.J. and Wilson, J.T., 2007. Appendix B: RCBA Chemical Database. Natural Attenuation of Fuels and Chlorinated Solvents in the Subsurface: 593-603.

Wüst, W.F., Köber, R., Schlicker, O. and Dahmke, A., 1999. Combined Zero- and First-Order Kinetic Model of the Degradation of TCE and cis-DCE with Commercial Iron. Environmental Science & Technology, 33(23): 4304-4309.

Yabusaki, S.B. et al., 2011. Variably saturated flow and multicomponent biogeochemical reactive transport modeling of a uranium bioremediation field experiment. Journal of Contaminant Hydrology, 126(3–4): 271-290.

Yeh, W.W.G., 1986. Review of Parameter Identification Procedures in Groundwater Hydrology: The Inverse Problem. Water Resour. Res., 22(2): 95-108.

Yoon, H., Hart, D.B. and McKenna, S.A., 2013. Parameter estimation and predictive uncertainty in stochastic inverse modeling of groundwater flow: Comparing null-space Monte Carlo and multiple starting point methods. Water Resources Research, 49(1): 536-553.

Zheng, C. and Wang, P.P., 1999. MT3DMS: a modular three-dimensional multispecies transport model for simulation of advection, dispersion, and chemical reactions of contaminants in groundwater systems; documentation and user's guide, DTIC Document.

Highlights

- A multicomponent reactive transport model of a real PRB site was developed.
- Heterogeneous aquifer properties were parameterized with pilot points.
- A stepwise approach for inversion of reactive transport was proposed.
- Reducing the amount of infiltrating rainwater avoids excessive contaminant dilution.
- Infiltration and hydraulic conductivity estimates must be validated on site.